Mixing and ageing in the polar lower stratosphere in winter 2015/2016

Jens Krause[1], Peter Hoor[1], Andreas Engel[2], Felix Plöger[3], Jens-Uwe Grooß[3], Harald Bönisch[2,4], Timo Keber[2], Björn-Martin Sinnhuber[4], Wolfgang Woiwode[4], and Hermann Oelhaf[4]

[1]Institute for Atmospheric Physics, Johannes Gutenberg-University of Mainz, Germany
[2]Institute for Atmospheric and Environmental Sciences, University of Frankfurt, Germany
[3]Institute of Energy and Climate Research (IEK-7), FZ Jülich, Germany
[4]Institute of Meteorology and Climate Research (IMK), Karlsruhe Institute of Technology (KIT), Germany

Correspondence to: Jens Krause (krauseje@uni-mainz.de)

Abstract. We present data from winter 2015/2016, which were measured during the POLSTRACC (The Polar Stratosphere in a Changing Climate) aircraft campaign between December 2015 and March 2016 in the Arctic upper troposphere and lower stratosphere (UTLS). The focus of this work is on the role of transport and mixing between aged and potentially chemically processed air masses from the stratosphere with mid and low latitude air mass fractions with small transit times originating at the tropical lower stratosphere. By combining measurements of CO, N_2O and SF_6 we estimate the evolution of the relative contributions of transport and mixing to the UTLS composition over the course of the winter.

We find an increasing influence of aged stratospheric air partly from the vortex as indicated by decreasing N_2O and SF_6 values over the course of winter in the extratropical lower and lowermost stratosphere between $\Theta = 360$ K and $\Theta = 410$ K over the North Atlantic and the European Arctic. Surprisingly we also found a mean increase of CO by (3.00 ± 1.64) ppb_V from January to March relative to N_2O in the lower stratosphere. We show that this increase of CO is consistent with an increased mixing of tropospheric air as part of the fast transport mechanism in the lower stratosphere surf zone. The analysed air masses were partly affected by air masses which originated at the tropical tropopause and were quasi-horizontally mixed into higher latitudes.

This increase of the tropospheric air fraction partly compensates for ageing of the UTLS due to the diabatic descent of air masses from the vortex by horizontally mixed, tropospheric influenced air masses. This is consistent with simulated age spectra from the Chemical Lagrangian Model of the Stratosphere (CLaMS), which show a respective fractional increase of tropospheric air with short transit times lower than six months and a simultaneous increase of aged air from upper stratospheric and vortex regions with transit times larger than two years.

We thus conclude that the lowermost stratosphere in winter 2015/16 was affected by aged air from the upper stratosphere and vortex region. These air masses were significantly affected by increased mixing from the lower latitudes, which led to a simultaneous increase of the fraction of young air in the Arctic lowermost stratosphere by 6 % from January to March 2016.

1 Introduction

Uncertainties in the description of mixing introduce large uncertainties to quantitative estimates of radiative forcing which are on the order of 0.5 W m^{-2} (Riese et al., 2012). Therefore it is important to quantify the contribution of the dynamical processes which act on the distribution of tracers. The Arctic UTLS during winter is affected by diabatic descent from the stratosphere and quasi horizontal mixing by the shallow branch of the Brewer-Dobson circulation, which connects the tropical tropopause region with the high Arctic (e.g. Rosenlof et al., 1997; Birner and Bönisch, 2011). We present data from winter 2015/2016, which were measured during the POLSTRACC (The Polar Stratosphere in a Changing Climate) aircraft campaign between December 2015 and March 2016 in the Arctic upper troposphere and lower stratosphere (UTLS) (see Fig. 1).

The focus of this work is on the role of transport and mixing between aged and potentially chemically processed air masses from the stratosphere with mid and low latitude air mass fractions with small transit times originating at the tropical lower stratosphere. By combining measurements of CO, N_2O and SF_6 we investigate the evolution of the relative contributions of transport and mixing to the UTLS composition over the course of the winter. During winter the UTLS region (Fig. 1) at high latitudes is strongly affected by the evolution of the polar vortex. Diabatic descent in the polar stratosphere, which is strongest inside the polar vortex results as part of the Brewer-Dobson circulation (Brewer, 1949; Dobson, 1956) in mid and high latitudes as response to the breaking of planetary and gravity waves (Haynes et al., 1991; Plumb, 2002; Butchart, 2014) in the upper stratosphere and mesosphere. This downwelling leads to an increasing contribution of stratospheric air masses from the overworld (defined as the region, where isentropes are entirely located in the stratosphere (Hoskins, 1991)). Over the course of winter they contribute to the composition of the lower overworld ($\Theta < 420$ K), where our measurements took place, and the lowermost stratosphere (LMS) (Rosenfield et al., 1994) (defined as the region bounded by the 380 K isentrope and the extratropical tropopause (Holton et al., 1995)).

Air masses descending from the upper stratosphere and mesosphere chemically differ from the composition of the LMS, since they are potentially affected by ozone depleting catalytic cycles (Solomon, 1999). Since the air inside the polar vortex is largely isolated and exhibits a strong diabatic descent due to radiative cooling and the wave-driven Brewer-Dobson circulation this leads to an increased fraction of air masses with a high mean age of air in the UTLS of high latitudes (e.g. Engel et al., 2002; Ploeger et al., 2015).

The mean age of air is defined as the first moment of the transit time distribution (or the so-called age spectrum) (Hall and Plumb, 1994; Waugh et al., 1997). Mean age can be determined from the observation of long-lived tracers, which ideally have no sources or sinks in the stratosphere and of which the temporal evolution of the mixing ratio at the tropical tropopause is well known (Waugh et al., 1997). Notably, the mean age is a bad descriptor for the full age spectrum, which is highly skewed (e.g. Hall and Plumb, 1994) and sometimes even multimodal (Andrews et al., 1999; Boenisch et al., 2009). For the estimate of the potential chemical impact of species particularly with lifetimes on the order of weeks to only a few months the mean age is insufficient and the full spectrum is needed (Schoeberl et al., 2000), which is however only available under very idealized conditions (Schoeberl et al., 2005; Ehhalt et al., 2007).

Observations of SF_6, N_2O and CO_2 from the ER-2 aircraft show that the mean age at northern high latitudes at an altitude of

20 km is on the order of 4-6 years (Andrews et al., 2001; Engel et al., 2002). Satellite observations of SF_6 confirm this and show further a strong interannual variability of the mean age in northern high latitudes (Stiller et al., 2008, 2012; Haenel et al., 2015). The observations also indicate a potential transport of mesospheric air to lower altitudes (Engel et al., 2006b; Ray et al., 2017), which however strongly depends on the strength and persistence of the Arctic polar vortex during the individual winters.

In addition to diabatic descent inside and outside the polar vortex quasi-isentropic mixing from lower latitudes leads to a contribution of relatively young air to the UTLS. As a result a seasonal cycle of the chemical composition of the UTLS up to $\Theta = 430$ K establishes a relatively tropospheric character during northern summer / autumn and a more stratospheric characteristic in late winter/spring (Hegglin and Shepherd, 2007). The chemical composition and age structure of the extratropical UTLS (ExUTLS) are affected by the competing diabatic downwelling of aged air and rapid quasi isentropic mixing down to the tropopause (Hoor et al., 2005; Engel et al., 2006a; Boenisch et al., 2009; Garny et al., 2014). The region between $\Theta = 380$ K and the bottom of the tropical pipe around $\Theta = 450$ K (Palazzi et al., 2011) is a key region for the transition between these transport regimes. The $\Theta = 380$ K isentrope coincides with the tropical tropopause and is therefore directly affected by diabatic vertical transport of tropospheric air through the tropical transition layer (TTL) (Fueglistaler et al., 2009) into the stratosphere. Above $\Theta = 380K$ these air masses, which ascended through the TTL are rapidly mixed quasi horizontally by breaking planetary waves with air from high latitudes in addition to the shallow branch of the Brewer-Dobson circulation (Birner and Bönisch, 2011; Abalos et al., 2013). This rapid transport modifies the abundance of particularly water vapour and ozone in this region, which have seasonally varying isentropic gradients (Rosenlof et al., 1997; Randel et al., 2006; Hegglin and Shepherd, 2007; Pan et al., 2007; Ploeger et al., 2013).

In our study we focus on the transition of the tracer composition in the vortex affected UTLS region up to $\Theta = 410$K during winter 2015/2016. We will quantify the effects of quasi-isentropic mixing from the tropics and diabatic downwelling and its effect on the chemical composition as well as the evolution of the age spectrum and the mean age in this region.

2 Meteorological conditions during winter 2015/16

The early Arctic winter 2015/16 (November/December) was among the coldest winters in the lower stratosphere (LS) since 1948. These extreme cold conditions existed due to a strong and cold Arctic polar vortex which developed in November 2015 due to very low planetary wave activity in the stratosphere (Matthias et al., 2016). From late December 2015 to early February 2016 the temperatures at $\Theta = 490$ K decreased below 189 K. Therefore strong dehydration and denitrification were seen in low H_2O and HNO_3 volume mixing ratios, which finally led to a strong chlorine activation in early winter. Using MLS data the chemical influence of the vortex could be observed on isentropes below $\Theta = 400$ K (Manney and Lawrence, 2016).

The major final warming (MFW) (Manney and Lawrence, 2016) occurred on 5 March 2016 which led to a split of the vortex one week later. This early final warming was unusual, as only five other MFWs since 1958 appeared before middle of March. Due to this early warming air masses in the polar lower stratosphere were mixed with non-vortex air and prevented chemical ozone depletion reaching record low values during winter 2015/16 (Manney and Lawrence, 2016, and references therein).

The winter 2015/16 was characterised by an unprecedented anomaly of the quasi biannual oscillation (QBO) with a westerly

jet formed within the easterly phase in the lower stratosphere (Newman et al., 2016; Osprey et al., 2016). Since the QBO affects the zonal wind direction in the tropical lower stratosphere (Niwano et al., 2003) its strength and phase is crucial for stratospheric transport processes (Baldwin et al., 2001) and westerly phases are related to a strong and cold polar Arctic vortex (Holton and Tan, 1980).

Further the winter 2015/16 was also affected by a strong warm phase of the El-Niño Southern Oscillation (ENSO) (Chen et al., 2016; L'Heureux et al., 2017). Matthias et al. (2016) argue that the strong El-Niño weakened the 2016 Arctic vortex, while Palmeiro et al. (2017) found a connection of this ENSO event to the strong polar vortex and the easterly MFW.

3 Project overview and measurements

This work will address the evolution of composition, age structure and the influence of transport and mixing of air masses in the lower stratosphere. The composition of air masses inside the LS, which is affected by diabatic descent of upper stratospheric air masses, irreversibly mixed with younger air from the TTL, is analysed by combining measurements of in-situ data with model calculations of the Chemical Lagrangian Model of the Stratosphere (CLaMS) (McKenna et al., 2002; Grooß et al., 2014; Ploeger et al., 2015).

3.1 The POLSTRACC campaign 2015/16

The data presented in this study were obtained during the POLSTRACC (Polar Stratosphere in a Changing Climate) mission, which was part of the combined PGS (POLSTRACC/GW-LCYCLE/SALSA) framework. The main objectives of the POLSTRACC mission were the investigation of structure, composition and dynamics of the Arctic LMS and processes involving chemical ozone depletion and polar stratospheric clouds in the Arctic winter UTLS. In total 17 scientific flights were performed from December 2015 until end of March 2016 on board the new German research aircraft HALO (High Altitude Long Range) from Oberpfaffenhofen, Germany (48.05 °N, 11.16 °E) and Kiruna, Sweden (67.49 °N, 20.19 °E) covering the region from 25 °N to 87 °N and 24 °E to 80 °W (Fig. 2). Typical flight altitudes ranged from 10 km asl[1] to 14.5 km asl corresponding to potential temperatures in the stratosphere from $\Theta = 320$ K up to $\Theta = 410$ K. The total flight time was about 157 hours, of which 19 hours were spent in December 2015, 62 hours were spent from January to February and 76 from February to March, respectively. For this study we focus on Arctic measurements starting from Kiruna, which took place during two campaign phases, representing flights from 12. January 2016 to 02. February 2016 (phase 1) and from 26. February 2016 to 18. March 2016 (phase 2). For this work we use approximately 50 hours of measurements of those flights which were conducted to probe air masses above the extratropical transition region (ExTL) and underneath the polar vortex above PV = 7 PVU(1 PVU = 10^{-6} m^2 s^{-1} K kg^{-1}).

The research aircraft HALO is a modified business jet type Gulfstream G-550. It has a maximum range of 12500 km with a maximum altitude of 15.5 km and can carry up to 3 tons of scientific payload. The payload was a combination of different remote sensing (e.g. WALES lidar (Wirth et al., 2009; Fix et al., 2016), Väisälä RD 49 dropsondes and GLORIA limb sounder

[1] above sea level

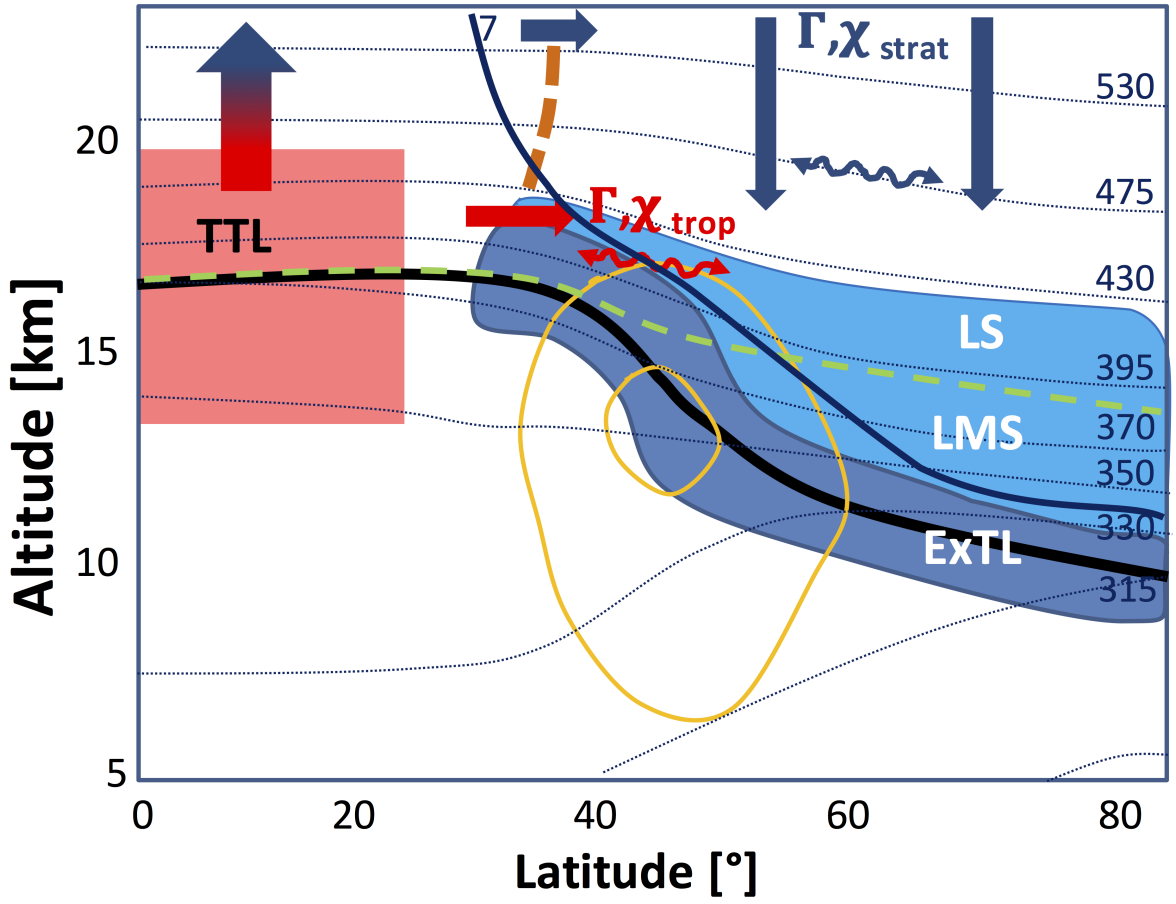

Figure 1. Cross section of the northern hemispheric UTLS (Upper Troposphere / Lower Stratosphere) region, adapted from Riese et al. (2014) and Müller et al. (2016). The thermal tropopause is denoted by the thick black solid line. The measurement region is depicted as blue box subdivided into the extratropical tropopause layer (ExTL), the lowermost stratosphere (LMS) and the lower stratosphere (LS). LMS and LS are separated by the 380 K isentrope (green dashed line). Transport pathways of air masses are denoted by coloured, thick arrows from the tropical tropopause layer (TTL) (red) and the polar Arctic upper stratosphere (blue) with respective mean age Γ and trace gas volume mixing ratio χ. Quasi horizontal mixing is represented by wavy double side arrows, indicating no net mass transport of air masses. Dotted lines are isentropes in K, the solid dark blue line indicates the 7 PVU contour, which is used to separate the regime of the ExTL from the LMS and LS (for details see text). Thin orange contour lines depict the zonal view of the jet stream.

(Friedl-Vallon et al., 2014; Kaufmann et al., 2015)) and in-situ instruments that measured trace gases with different lifetimes, sources and sinks.

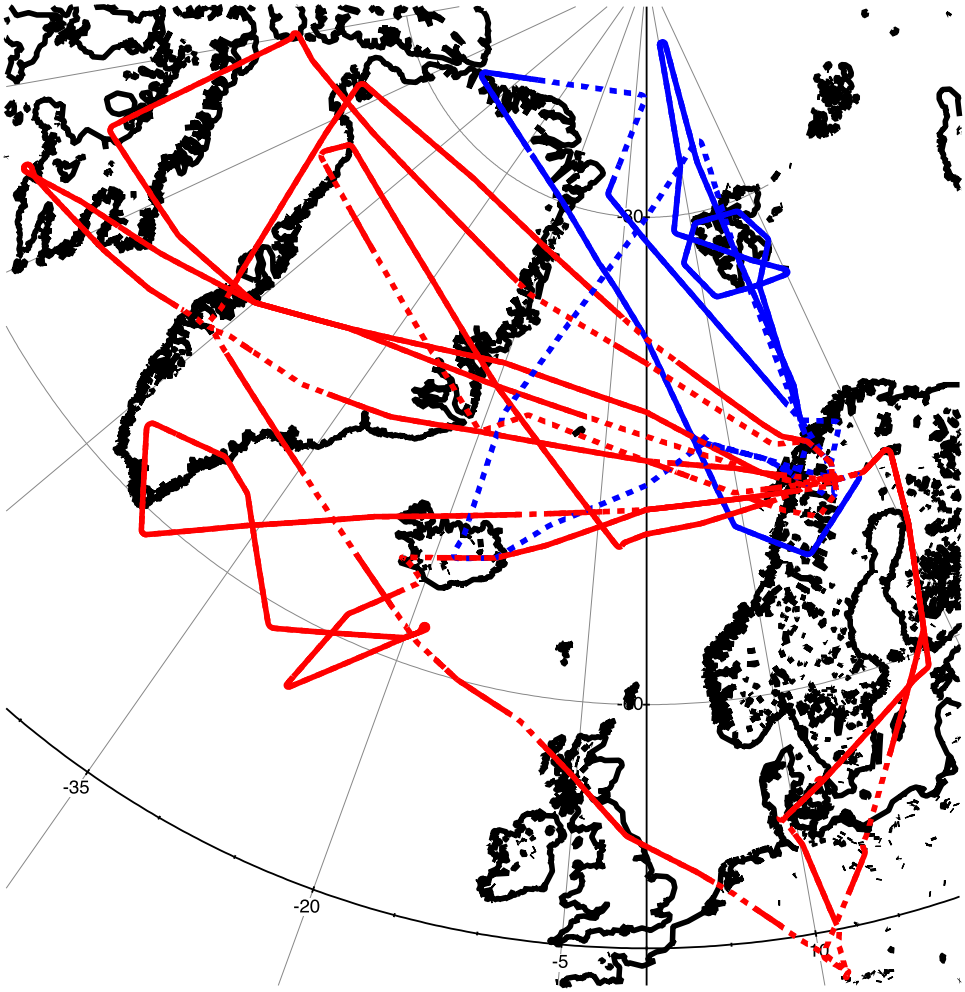

Figure 2. Flight tracks during the POLSTRACC campaign. Blue colours indicate flights during phase 1 (12. January-02. February), red colours indicate flights during phase 2 (26. February-18. March). Flights that were used for the analysis are shown as solid lines. Dotted lines denote flight legs with PV < 7 PVU. For details see Sect. 3.1.

3.2 In-situ trace gas measurements

In this study we analyse measurements of N_2O and CO, which were measured with the TRIHOP instrument (Müller et al., 2015) and SF_6 by the GhOST-MS instrument (Sala et al., 2014). For our analysis the data are synchronised to a common time resolution of 0.1 Hz, corresponding to a horizontal resolution of 2.5 km at typical HALO flight speeds. GhOST data is available with a resolution of 60 seconds at an integration time of one second which leads to a horizontal resolution of 15 km.

3.2.1 The TRIHOP instrument

The TRIHOP instrument (Schiller et al., 2008) is an infrared absorption laser spectrometer with three quantum cascade lasers (QCL) operating between wavenumbers 1269 cm^{-1} and 2184 cm^{-1} that measures CO, N_2O and CH_4. The instrument uses a multi-pass White cell with a constant pressure of 30 hPa to minimize pressure broadening of the absorption lines. The three species are subsequently measured with an integration time of 1.5 s per species during a full cycle which finally leads to a time resolution of 7 seconds due to additional latency times when the channels are switched. In flight calibration is performed against compressed ambient air standards that were calibrated against primary standards before and after the campaign. The primary standards are traceable to the World Meteorological Organisation Global Atmosphere Watch Central Calibration Laboratory (WMO GAW CCL) scale (X2007) for greenhouse gases. During POLSTRACC it was possible to achieve a (2σ) precision of CO, N_2O and CH_4 of 1.15, 1.84 and 9.46 ppb_V respectively.

3.2.2 GhOST-MS in-situ measurements

The GHOST-MS instrument is a two channel gas chromatograph for airborne measurements of trace gases. One channel uses a mass spectrometer (Agilent MSD 5975) for the detection of atmospheric trace gases at a time resolution of four minutes. This channel uses negative ion chemical ionization as described in Sala et al. (2014) to measure brominated hydrocarbons. The other channel measures SF_6 and CFC-12 using an ECD (Electron capture detector) with a time resolution of one minute. For the POLSTRACC campaign the precision for SF_6 was 0.6% and the precision for CFC-12 was 0.2%.

Mean age of air is inferred from SF_6 measurements (Engel et al., 2009). Due to its much higher atmospheric mixing ratio, the precision of CFC-12 measurements is better than that of SF_6 measurements. Prior to calculating mean age, the SF_6 time series has therefore been smoothed using the CFC-12, by applying a local (ten minutes of data before and after the time of measurement) fit between CFC-12 and SF_6. This procedure removes parts of the instrumental scatter but retains the local information, keeps particularly the atmospheric variability (unlike averaging) and does not introduce any offset to the mean age values. Mean age derived in this way has an overall precision of better than 0.3 years and an estimated accuracy of 0.6 years, as explained in Engel et al. (2006a). Both SF_6 and CFC-12 are reported on the SIO-2005 scale.

3.3 The Chemical Lagrangian Model of the Stratosphere (CLaMS)

The analysis of trace gas measurements is complemented by simulations with the Chemical Lagrangian Model of the Stratosphere CLaMS (McKenna et al., 2002; Konopka et al., 2004). CLaMS is a Lagrangian chemistry transport model, based on forward trajectory calculations and a parameterization of small-scale atmospheric mixing which depends on the deformation rate of the large-scale flow. The model simulation is driven with meteorological data (e.g., horizontal wind fields) from European Center of Medium Range Weather Forecasts (ECMWF) ERA-Interim reanalysis (Dee et al., 2011) and covers the period 1979-2017. The model uses an isentropic vertical coordinate throughout the stratosphere and the vertical velocity is deduced from the reanalysis total diabatic heating rate. Further details about the model set-up and the included chemical reactions (relevant species here are CO and N_2O) are given in Pommrich et al. (2014). This long-term CLaMS simulation has been shown to reliably represent transport processes in the lower stratosphere for the relevant trace gas species CO and N_2O (Pommrich et al., 2014) as well as for mean age of air (Ploeger et al., 2015).

Recently, a method to calculate the age of air spectrum has been implemented in CLaMS (Ploeger and Birner, 2016), which will be used in the following analysis. The age spectrum is the transit time distribution of air masses for transport from a control surface (usually taken as the tropical tropopause or the Earth's surface) to a given location in the stratosphere (e.g. Hall and Plumb, 1994; Waugh, 2002) and can be related to the Green's function of the transport equation. The calculation method in CLaMS is based on inert tracer pulses, with different tracers released every other month at the surface in the tropics. This method allows the calculation of time dependent age spectra for the non-stationary atmospheric flow at any location and time in the model domain (see Ploeger and Birner (2016) for further details). Mean age in CLaMS is calculated from an inert model "clock-tracer" with linear increasing mixing ratio at the surface (Hall and Plumb, 1994). The resulting mean ages are fully consistent with mean age calculated as the first moment of the CLaMS age spectrum (Ploeger and Birner, 2016).

A CLaMS simulation with full stratospheric chemistry was integrated as described by Grooß et al. (2014). The upper boundary is set to Θ =900 K potential temperature, where tracers like O_3, N_2O and CO are constrained by MLS satellite observations. Due to its Lagrangian formulation, a box-trajectory model setup is also possible in which the identical chemistry scheme is used along single air mass trajectories. This setup is also used here to diagnose chemical pathways and chemical conversion rates. This box model setup is also used here to estimate CO production and loss rates.

4 Results

As shown in Hoor et al. (2010) rapid and frequent mixing with tropospheric air mainly affects the region of PV < 7 PVU. To exclude mixing with air masses of recent tropospheric origin or from the exTL (extratropical tropopause layer) we only selected data above this level of potential vorticity. Therefore the composition of analysed data is mainly affected by isentropically, irreversibly mixed air mass signatures originating out of the tropics and diabatically descended air masses from the upper stratosphere in the polar region. In this analysis we further excluded flights, which were dedicated to the observation of gravity waves.

4.1 Tracer distributions and mean age

Figures 3, 4 and 5 show tracer distributions as a function of equivalent latitude and potential temperature θ (Strahan et al., 1999; Hoor et al., 2004; Hegglin et al., 2006). Equivalent latitude is directly linked to the potential vorticity, which is conserved under adiabatic processes (Holton, 2004). Therefore, these coordinates are suitable to account for reversible adiabatic tracer transport.

4.1.1 Age of air

An air parcel in the stratosphere is a mixture of fractions of air with different histories, transport pathways and individual transit times. The transport pathways create an age spectrum or transit time distribution. The age spectrum can be obtained by calculation of the Green's function of the tracer continuity equation for a conserved and passive species (Hall and Plumb, 1994).

The mean age is defined as the first moment of the transit time distribution. To determine the mean age from long-lived tracer measurements, the tracer must have a well known source distribution at the tropical tropopause and a well defined vertical gradient in the stratosphere (Hall and Waugh, 1997). Since SF_6 is a long-lived inert trace gas with a well known increase of its mean surface mixing ratio, it is commonly used for calculations of mean age (Boenisch et al., 2009). The sink of SF_6 is in the mesosphere, where it is destroyed by shortwave UV radiation. The lifetime of SF_6 is assumed to be 3200 years, but recent studies indicate a significantly shorter lifetime of about 850 years (Ray et al., 2017). This implies that mean age derived from SF_6 may be too old. Models and observations both show a high bias of up to one year in the polar vortex (Ray et al., 2017) or even more in mesospheric air (Engel et al., 2006b). Since we focus on the lower stratosphere far below the mesospheric loss region for SF6 and we further focus on age changes our data are not affected by this fact.

Figure 3 a) and b) show the distribution of mean age calculated from SF_6 measurements for phase 1 (January) and phase 2 (February / March). Panel (a) shows that the LS during phase 1 is dominated by air masses of mean ages between 0.5 years to less than three years at maximum. The oldest air masses with mean ages older than two years were encountered at largest distances from the tropopause and potential temperatures ranging from $\Theta = 360$ K to $\Theta = 380$ K. In contrast, during phase 2 (panel (b)) in general much older air masses up to five years were found at potential temperatures of $\Theta = 410$ K. These higher potential temperatures at flight altitude are the result of the diabatic descent over the course of winter and indicate an increasing influence of air masses originating deeper in the stratosphere or from the Arctic polar vortex. To directly compare the temporal evolution of the age of air in the lower stratosphere panel (c) shows the difference of age of air between both phases and shows that the bulk of air inside the LS is getting older between $\Theta = 330$ K and $\Theta = 380$ K. The mean increase is 0.29 years, indicating diabatic downwelling due to the evolution of the polar vortex and thus an increased mean age in late winter.

4.1.2 Nitrous oxide

Nitrous oxide (N_2O) has a lifetime of 123 years (Ko et al., 2013) and is released at the surface with no chemical sources in the atmosphere (Dils et al., 2006). As a result N_2O has a near constant tropospheric value of 329.3 ppb_V (winter 2015/2016 ac-

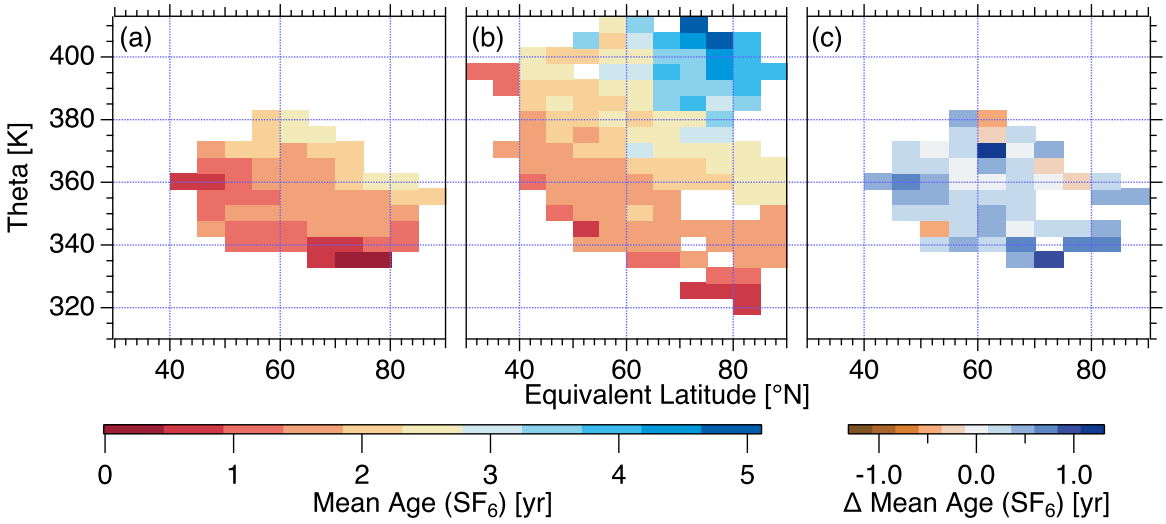

Figure 3. Distributions of mean age from SF_6 measurements in potential temperature - equivalent latitude coordinates for PV > 7 PVU. Panel (a) shows data for phase 1, (b) for phase 2 and panel (c) shows their absolute difference (phase 2-phase 1). The colour code represents the mean age. Blue colours in panel (c) indicate an increase of mean age in the subvortex region from January to March. Only bins with more than ten data points are shown.

cording to NOAA) that makes stratospheric influence identifiable (Müller et al., 2015). The mean annual tropospheric increase is currently approximately 0.78 ppb_V per year (Hartmann et al., 2013).

The main sink reactions of N_2O are due to photolysis in the UV-band (190 nm $\leq \lambda \leq$ 220 nm) and the reaction with $O(^1D)$ which only occurs within the upper stratosphere (Ko et al., 2013). Thus, N_2O above the tropopause shows a weak negative vertical gradient which maximizes during winter and spring due to the diabatic downwelling by the Brewer-Dobson circulation. Figures 4 a) and b) show N_2O values between 276 and 325 ppb_V measured during phase 1 and values below 200 ppb_V measured during phase 2 above Θ = 400 K. Figure 4 c) shows an overall decrease in N_2O in the polar lower stratosphere due to diabatic descent during winter, consistent with mean age changes (Fig. 3 c)).

4.1.3 Carbon monoxide

Carbon monoxide (CO) is released to the atmosphere mainly through incomplete combustion processes and methane oxidation as the only significant in-situ source. Due to the high variability of anthropogenic surface emissions, CO mixing ratios in the nothern hemisphere vary from 70 ppb_V to 200 ppb_V (Prinn et al., 2000) and the CO lifetime is on the order of weeks. In the lower stratosphere the main source of CO is the methane oxidation with the OH radical. The main sink is oxidation by OH. The CO lifetime during polar night is a few months. In the stratosphere CO is controlled by production from methane oxidation and CO

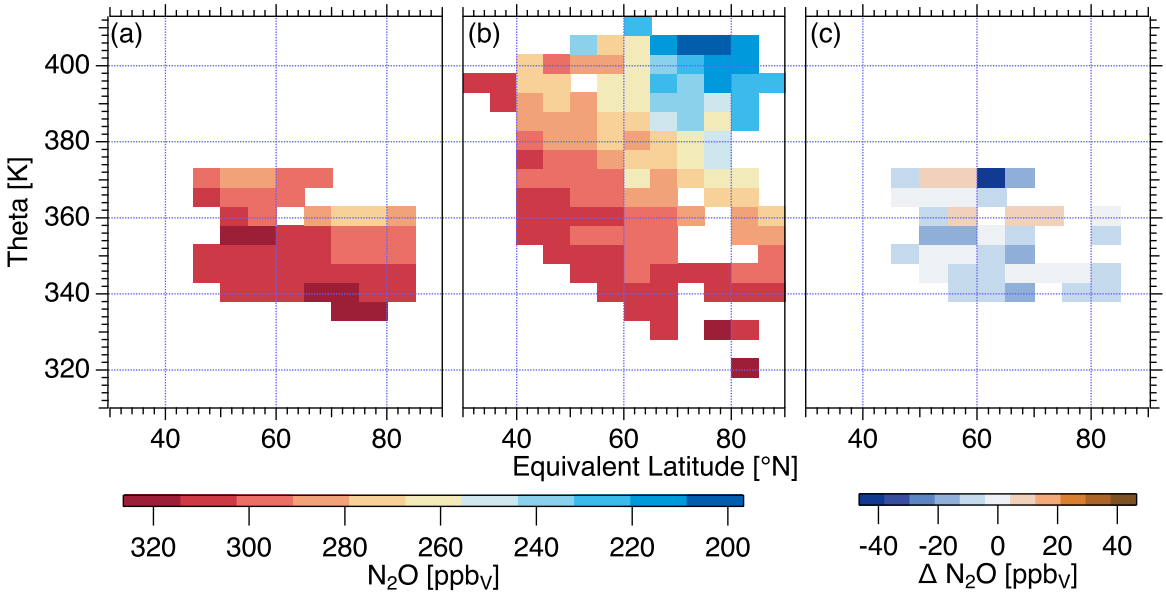

Figure 4. As Fig. 3 but for N_2O. Negative (blue) values in panel (c) indicate an overall decrease of N_2O in the measurement region in accordance with increasing mean age (Fig. 3c).

degradation. In the absence of transport from the troposphere this leads to an equilibrium between production and destruction of CO. We found an equilibrium value of 10-15 ppb_V in winter 2015/2016, depending on the integrated temperature history of the respective air mass in agreement with previous studies (Müller et al., 2016; Herman et al., 1999).

The reaction of CH_4 with Cl is an insignificant source of CO in the lower stratosphere (Flocke et al., 1999). Transport from the mesosphere, where CO is produced from the photolysis of CO_2, also provides a potential source of CO via strong diabatic descent during winter under persistent polar vortices (Engel et al., 2006a). These potential influences are discussed in chapter 6.

Figure 5 shows the distribution of CO. During phase 2 (panel (b)) the lowest mixing ratios of 15 ppb_V were found at potential temperatures between $\Theta = 380$ K and $\Theta = 410$ K and equivalent latitudes > 60 °N. As can be seen by the vertical branch of the CO-N_2O correlation (Fig. 6 and 7), this value is the stratospheric equilibrium during late winter. Phase 1 (panel (a)) values ranged between 60 ppb_V and 17 ppb_V, hence the stratospheric background value was not measured in January 2016. A strong tropospheric influence is evident below $\Theta = 340$ K with CO values up to 57 ppb_V at phase 1 and 47 ppb_V at phase 2. Hence the overall distribution of carbon monoxide in the UTLS during the individual phases (Fig. 4 a) and b))seems to be consistent with N_2O and mean age obtained from SF_6 measurements, despite its much shorter lifetime compared to the other species.

However, when comparing the differences of the respective phases (panel c), we see a different behaviour compared to N_2O and SF_6. We encountered an increase of carbon monoxide mixing ratios over the course of winter, which is at first glance in contradiction to the distributions of mean age and N_2O. While the distributions of long-lived tracers SF_6 and N_2O indicate an

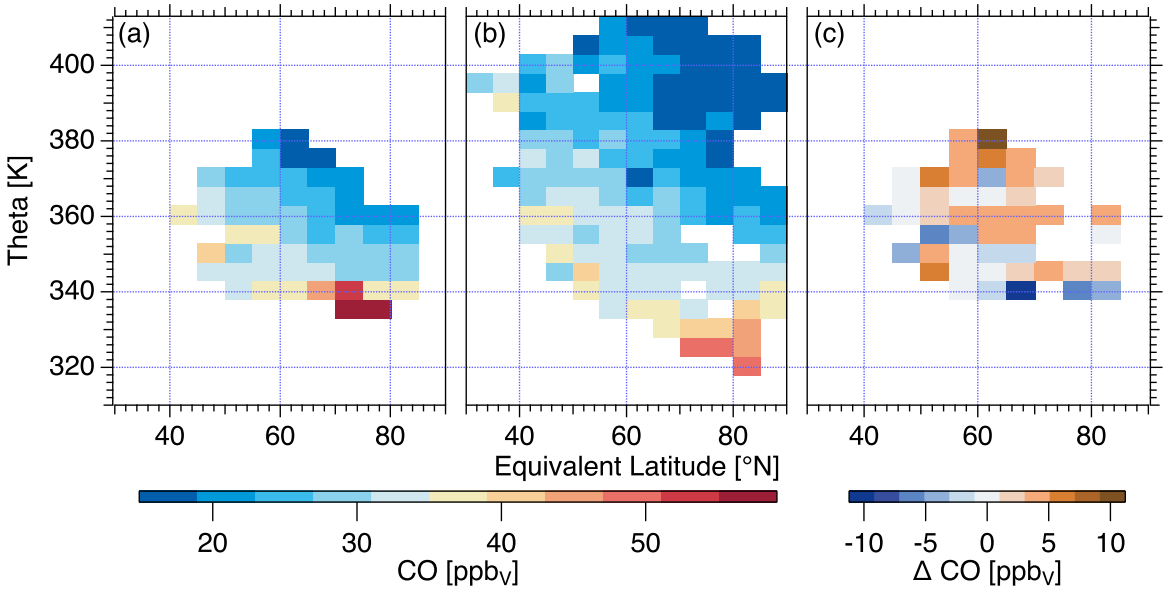

Figure 5. As Fig. 3 and Fig. 4 but for CO. Note the positive difference of CO in panel (c) indicating an increase of CO in the measurement region.

ageing of air masses, the increase of short-lived CO indicates a source of CO either from the troposphere or the stratosphere. Note that the increase is observed above $\Theta = 360$ K and 50 °N equivalent latitude. Below $\Theta = 360$ K decreasing values are encountered. We will analyse the potential sources of CO in the following and suggest that CO increases due to an enhancement of mixing of tropospheric air from the tropical lower stratosphere over the course of the winter without an increase of the upper tropospheric mixing ratios, which are affected by the surface emissions.

5 Analysis

We found a decrease of the long lived species SF_6 and N_2O with their lowest values far above the local troposphere in late winter, which fits well in the general picture of enhanced downwelling of the Brewer-Dobson circulation in late winter/spring. The unexpected, simultaneous increase of the short lived CO over the course of winter could indicate a strengthening of tropospheric transport by enhanced mixing with air from the tropical lower stratosphere. In the following we will discuss this hypothesis and also other potential sources for the additional CO mixing ratios.

5.1 Identification of mixing on the basis of tracer-tracer correlations

To identify mixing processes across the tropopause CO-O_3 correlations have been widely used (Fischer et al., 2000; Zahn et al., 2000; Hoor et al., 2002; Pan et al., 2004; Müller et al., 2016). Since ozone is affected by chemical processes particularly in

the vortex region we use N_2O as a stratospheric tracer instead of ozone. Carbon monoxide, used here as a tropospheric tracer also has sources in the mesosphere and via chlorine chemistry in the stratosphere. In the LS the influence of chlorine is small, compared to the reaction with the hydroxyl radical, therefore we investigated the influence of chlorine chemistry regarding methane which leads to the formation of CO. This influence will be discussed in detail later.

To analyse the effects of transport and mixing on the evolution of the UTLS composition we used the N_2O-CO relation as shown in Fig. 6. Tropospheric data have high N_2O values (> 328 ppb_V) and are accompanied by high CO values, while stratospheric data have N_2O < 328 ppb_V. Due to the tropospheric background value of N_2O and the stratospheric equilibrium of CO, the troposphere can be identified as horizontal (high amount of N_2O, variable CO) branch and the stratosphere, free of tropospheric influence can be identified as vertical branch (low amount of CO, variable N_2O) of the correlation. Without any recent mixing, the tracer-tracer correlation of N_2O and CO would form an L-shape structure (Fischer et al., 2000). In the presence of rapid mixing a straight mixing line between two end members of the correlation is established (panel a) (Hoor et al., 2002; Müller et al., 2016). As stratospheric CO will relax towards its stratospheric equilibrium value while N_2O is long-lived in the lower stratosphere, the initial linear correlation will become curved with time in case of inefficient mixing when the chemical lifetime is shorter than the time scale of mixing (panel b). Depending on the strength of mixing relative to the chemical CO sink the curvature will change and is less pronounced as the mixing gets more efficient (panel c). It is important to note that the change of CO relative to a given N_2O value can only be explained by a change of the ratio between mixing and chemical time scales. Mixing alone acts on both tracers N_2O and CO. Therefore a change of the shape of the curve is a direct result of the increased mixing relative to the chemical timescale, which is less efficient when mixing becomes stronger. Panel (d) of Fig. 6 shows additionally the correlation under mesospheric influenced conditions. In this case the correlation would rise to higher CO mixing ratios and lower N_2O mixing ratios, since N_2O gets destroyed and CO produced in the mesosphere.

Figure 7 shows the N_2O-CO correlation for POLSTRACC separated for phase 1 and phase 2, respectively binned in intervals of 5 ppb_V N_2O. It is evident that mixing of tropospheric and stratospheric air masses occurs in both phases. During phase 1 (blue curve) CO ranges between 20 ppb_V and 60 ppb_V at N_2O values between 323 ppb_V and 270 ppb_V. Notably the red curve (phase 2) shows a steeper gradient with CO values between 43 ppb_V and 15 ppb_V at N_2O values between 323 ppb_V and 180 ppb_V. There are higher CO mixing ratios for N_2O values lower than 310 ppb_V in the later phase 2 of the measurements. Additionally the red curve tends towards a CO equilibrium value of 15.67 ppb_V for N_2O values in the range of 220 ppb_V to 180 ppb_V.

Most importantly, there is an increase of CO on N_2O isopleths between 313 ppb_V and 273 ppb_V N_2O over the course of winter. This is a remarkable result since we expect that due to the ageing of air inside the lower stratosphere in winter, the CO mixing ratio decreases with time. It is important to note that the correlation along the mixing line which connects tropospheric values with the stratosphere shows higher CO relative to N_2O in phase 2. As indicated in Fig. 6 this is a clear indication for enhanced mixing of tropospheric air masses for N_2O values > 273 ppb_V. Furthermore phase 1 shows higher CO values relative to N_2O compared to phase 2 for N_2O values larger than 313 ppb_V. Therefore we can conclude that regarding the CO-N_2O correlation the tropospheric impact on short timescales through the ExTL was greater in phase 1 than in phase 2, indicating enhanced mixing with tropospheric influenced air originating in the TTL region during phase 2.

A potential mesospheric impact is highly unlikely due to the fact that during phase 2 the N_2O-CO correlation tends towards

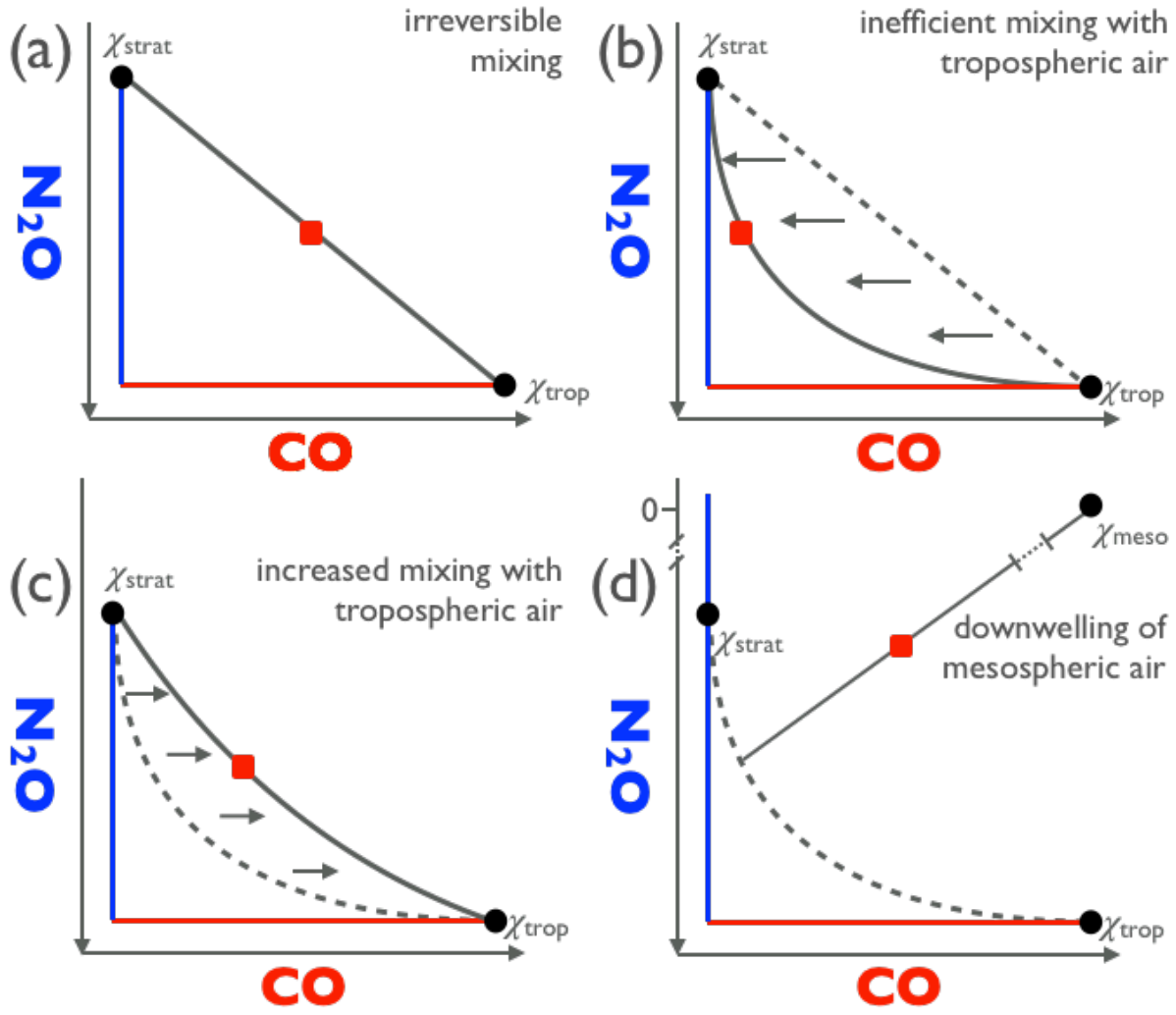

Figure 6. Sketch of tracer-tracer correlations with different lifetimes. Note that the N_2O axis is reversed. Panel (a) shows the L-shape structure with an air parcel (red box) on a straight mixing line for fast mixing timescales. The horizontal red line represents the tropospheric N_2O background, the blue vertical line the stratospheric CO equilibrium. Panel (b) shows the resulting curve in case of inefficient mixing compared to the chemical lifetime. Panel (c) shows the change of curvature, depending on the strength of mixing and panel (d) shows the influence of the mesosphere on the correlation.

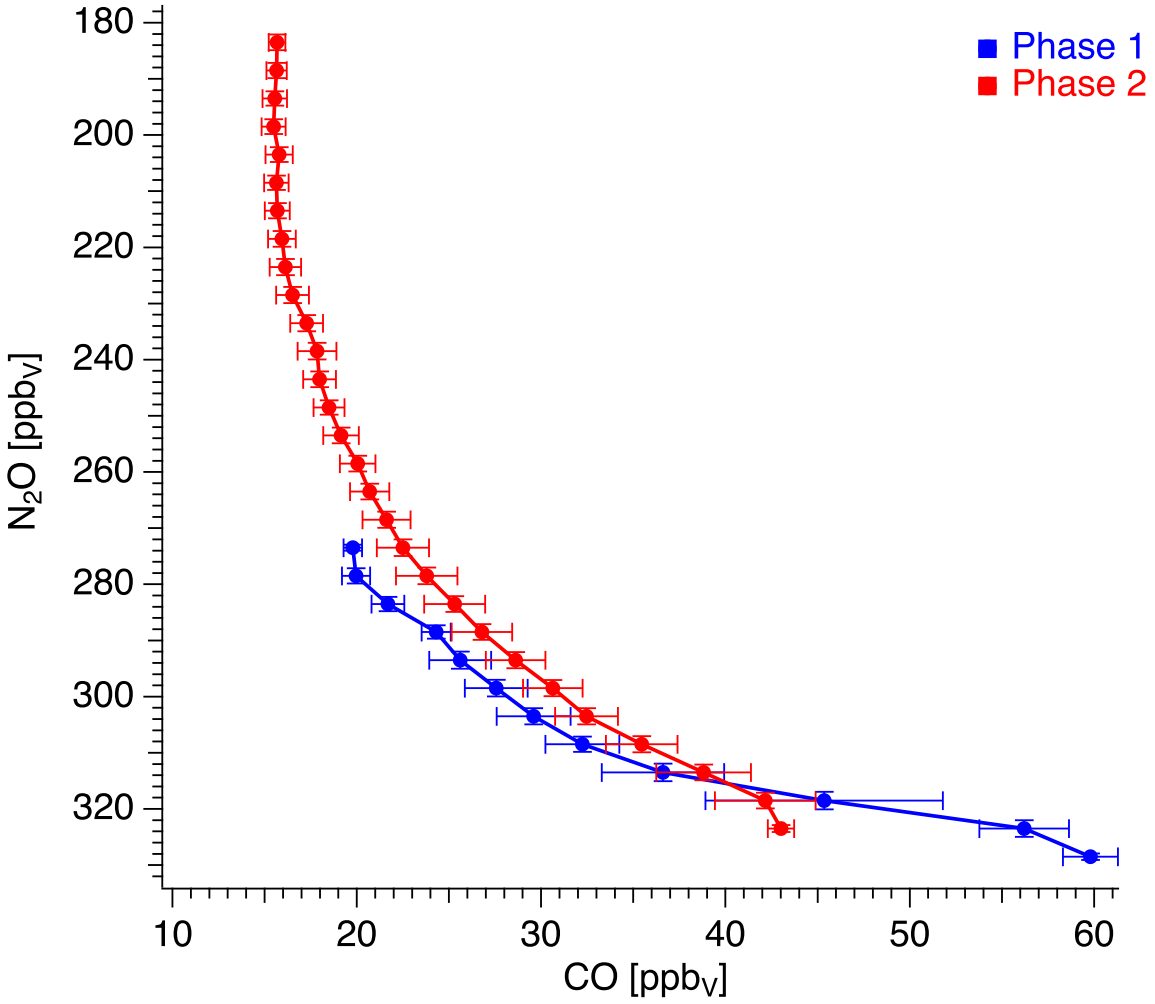

Figure 7. N_2O-CO correlation for POLSTRACC flights with PV > 7 PVU. The blue curve represents phase 1, the red curve represents phase 2. Data are binned in steps of 5 ppb_V N_2O. The variability in each bin is given by the vertical and horizontal lines, respectively.

the equilibrium value in the region of lower N_2O values. This influence will be discussed later in detail.

During both phases the UTLS between $\Theta = 340$ K and $\Theta = 380$ K was covered by our measurements. Therefore we assume the TTL (Fueglistaler et al., 2009) region (Fig. 1), where most of the tropospheric air masses are transported into the stratosphere (Schoeberl et al., 2006, and references therein) is the main source for the enhanced CO values (Fig. 5 panel (c)). Further on, rapid eddy mixing of air from the TTL leads to an increase of tropospheric tracer signatures in the Arctic region (Rosenlof et al., 1997).

To quantify the increasing influence from tropospheric air masses in the lower stratosphere, we applied a simple mass balance approach to quantify the composition of the lower stratosphere. Therefore, we assume an air parcel in the lower stratosphere may consist of either upper stratospheric or tropospheric origin (Fig. 1). This mass balance system is solved to get the amount of tropospheric fraction f_{trop} of the measured air.

For a mixing ratio χ on a specific isentrope θ we assume

$$\chi(\theta) = f_{\text{trop}} \cdot \chi_{\text{trop}} + f_{\text{strat}} \cdot \chi_{\text{strat}} \tag{1}$$

and

$$f_{\text{trop}} + f_{\text{strat}} = 1 \tag{2}$$

which leads to the tropospheric fraction f_{trop} based on CO measurements

$$f_{\text{trop}} = \frac{\chi_{\text{CO,m}} - \chi_{\text{CO,strat}}}{\chi_{\text{CO,trop}} - \chi_{\text{CO,strat}}} \tag{3}$$

with $\chi_{\text{CO,m}}$ the measured CO mixing ratio, $\chi_{\text{CO,strat}}$ the stratospheric CO background which was set to 15.7 ppb_V as mean of the vertical branch of the CO-N_2O correlation and $\chi_{\text{CO,trop}}$ the tropospheric CO entry value in the TTL.
In-situ measurements have shown that CO mixing ratios above the tropical tropopause are at levels between 50 and 60 ppb_V (Herman et al., 1999; Marcy et al., 2007).

Figure 8 shows the difference of the calculated tropospheric fraction f_{trop} between phase 2 and phase 1 as a function of N_2O, which acts as a quasi vertical coordinate. The CO increase over the course of winter corresponds to an increase by f_{trop} of $(6.8 \pm 3.7)\%$ between 313 ppb_V and 273 ppb_V N_2O by assuming 60 ppb_V of CO at the tropical tropopause as provided by in-situ aircraft data from Herman et al. (1999); Marcy et al. (2007). Using CO_{trop} = 80 ppb_V as indicated by MLS at 100 hPa one obtains 32 $\%$ lower values for f_{trop}, which is still a significant increase of tropospheric air masses. Note that additionally the tropospheric fraction decreases towards more tropospheric N_2O values from phase 1 to phase 2. This is a clear evidence that an increase of the CO mixing ratio at the tropopause is not the cause for the observed lower stratospheric CO increase. This would be consistent with an increase of the fraction of young air of tropospheric origin and more efficient mixing as indicated in Fig. 6. Panel (b) shows the distribution against equivalent latitude. Note that the observed increase is most prominent above $\Theta = 360$ K. This is a clear indication that mixing at $\Theta < 360$ K is suppressed due to the strong subtropical jet, which acts as a barrier for mixing (Haynes and Shuckburgh, 2000) and would be consistent with enhanced mixing out of the TTL region.

5.2 Age spectra analysis

For further analysis of the relationship between diabatically descended, aged air with longer transit times and potentially mixed with young tropospheric air with shorter transit times we use age spectrum calculations of the CLaMS (Chemical Lagrangian Model of the Stratosphere) (McKenna et al., 2002; Ploeger et al., 2015; Ploeger and Birner, 2016) model, which gives information on the full transit time distribution. Notably we have the age spectral information for each individual data point along

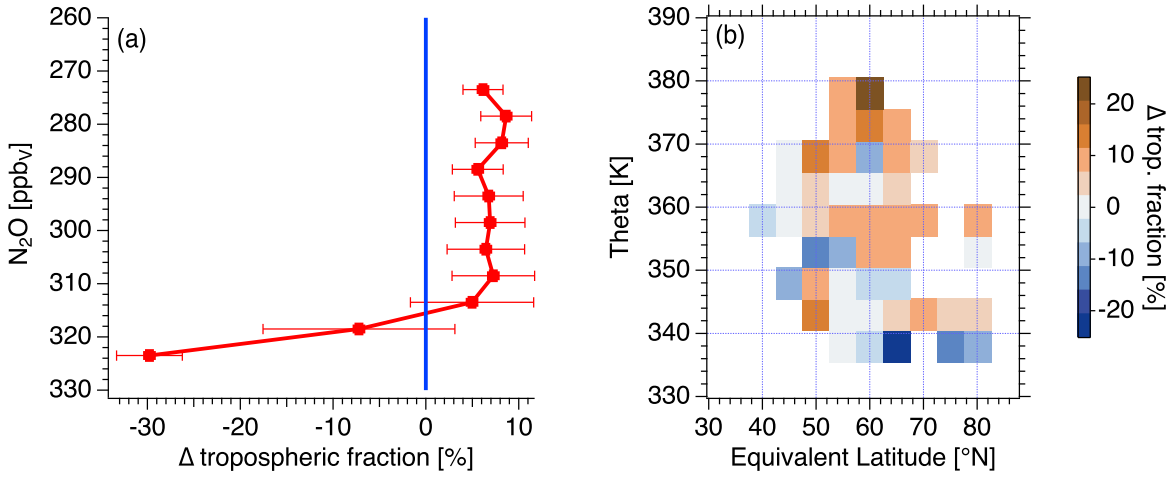

Figure 8. Panel (a): Tropospheric CO fraction from the mass balance equation as a function of N_2O showing the difference between phase 2 and phase 1. Panel (b): The same as (a) but as distribution against equivalent latitude. Red colours indicate an increase of the tropospheric CO fraction.

the flight track and therefore can directly compare our measurements with the spectrum.

To test if the model is able to reproduce the observations of tracers we compared CO and N_2O from CLaMS with the measurements (Fig. 9). Model output is available along the flight track with a time resolution of ten seconds. Figure 9 shows the N_2O-CO scatter plot for each data point. Panel (a) shows the correlation measured with the TRIHOP instrument, panel (b) shows the correlation calculated out of the CLaMS model. As is evident CLaMS correctly represents the increase of CO relative to N_2O from phase 1 to phase 2. Also the separate branches of the two phases are reproduced and the crossing of the correlation at 40 ppb_V CO and 310 ppb_V N_2O is consistently simulated.

This remarkable agreement between model and observations further motivates the usage of CLaMS for age analysis of our measurements.

As mentioned before, CLaMS is able to calculate the full transit time distribution of analysed air masses for each individual data point along the flight track. Figure 10 shows the averaged age spectra of the CLaMS model for the respective phase (panel (a)) and their difference (panel (b)). Vertical solid lines represent the mean age of the respective phase (blue and red) calculated by the CLaMS model, the dashed vertical lines separate young air masses with a mean age lower than 0.5 years and old air masses with mean age larger than 2 years. Since we have the full transit time distribution of each data point, we can compare this relation between the different parts of the age spectrum. An increase of the tropospheric fraction would be linked to an increase of the part of the age spectrum with low transit times as indicated by the observed increase of CO relative to N_2O.

Figure 10 shows an absolute increase of air masses older than two years up to 0.3% per month. For air masses younger than six months, there is also an increase of the age spectrum between phase 2 and phase 1 evident, with maximum values up to 0.9% per month, larger than the increase of the old air masses. The relative change of air masses younger than six months is

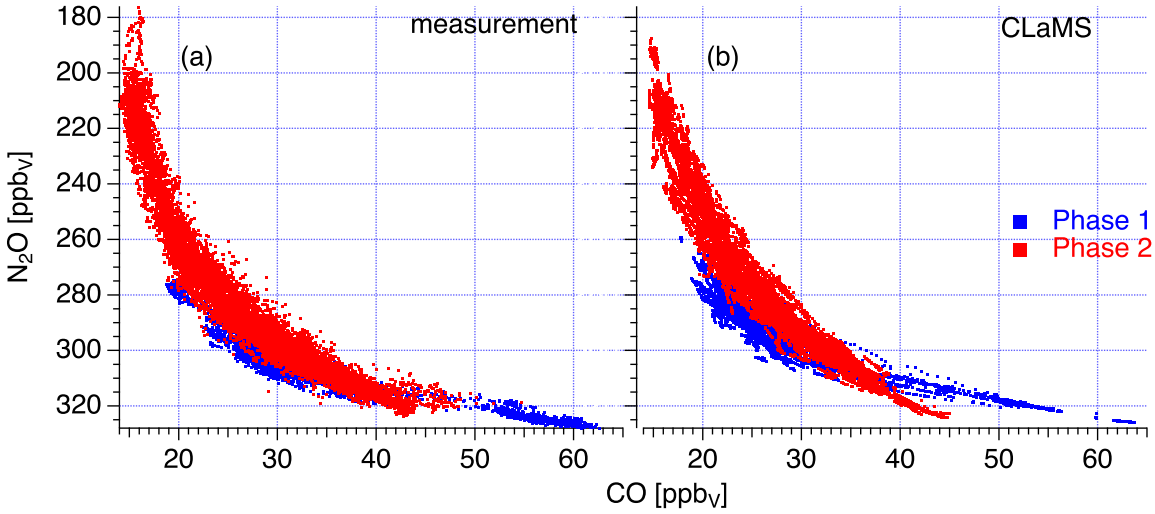

Figure 9. N_2O-CO scatter plot measured by the TRIHOP instrument (a) and CLaMS model output (b). Phase 1 coloured in blue, phase 2 coloured in red. The model output is available along the flight track with a time resolution of ten seconds.

19.5 % and for air masses older than two years 76.4 %. The increase of the young fraction is in agreement with the observed CO increase, indicating increased mixing with air from the TTL at the end of winter.

Since the mean age is calculated as the first moment of the distribution its value is most sensitive to changes in the old tail of the distribution (Hall and Waugh, 1997). Therefore the mean age rises by 0.27 years from 1.71 years to 1.98 years as a result of the increase of the age spectrum distribution for air masses older than two years. This matches the mean age increase of SF_6 and indicates, in agreement with the decrease of N_2O, the overall ageing in the lower and lowermost stratosphere over the course of winter. Since the integral over the Green's function is normalised to one, the increases of air masses older than two years and younger than six months must result in a relative decrease in between. Therefore air masses with mean ages between 0.5 years and 2 years are more enhanced in phase 1 than in phase 2, which is evident by the change of the transit time distribution up to -1.9% per month.

To further investigate the relationship of young versus aged air, we calculated the accumulated fraction of air masses with transit times lower than six months and older than two years for each data point. Figure 11 shows the binned fraction of air masses with transit times lower than six months versus the modelled mean age.

The comparison of the scatter plot for different times (phase 1 and phase 2) shows that for a given mean age a significant increase of the young tropospheric contribution is evident. Thus, according to the model and in agreement with the observed increase of CO, the late winter LS is more affected by tropospheric young air. Therefore our results demonstrate, that the mean age is an incomplete descriptor when referring to chemical properties of air masses involving different chemical life times of species. Since the mean age is just a single number it might be insensitive to changes of the processes and time scales

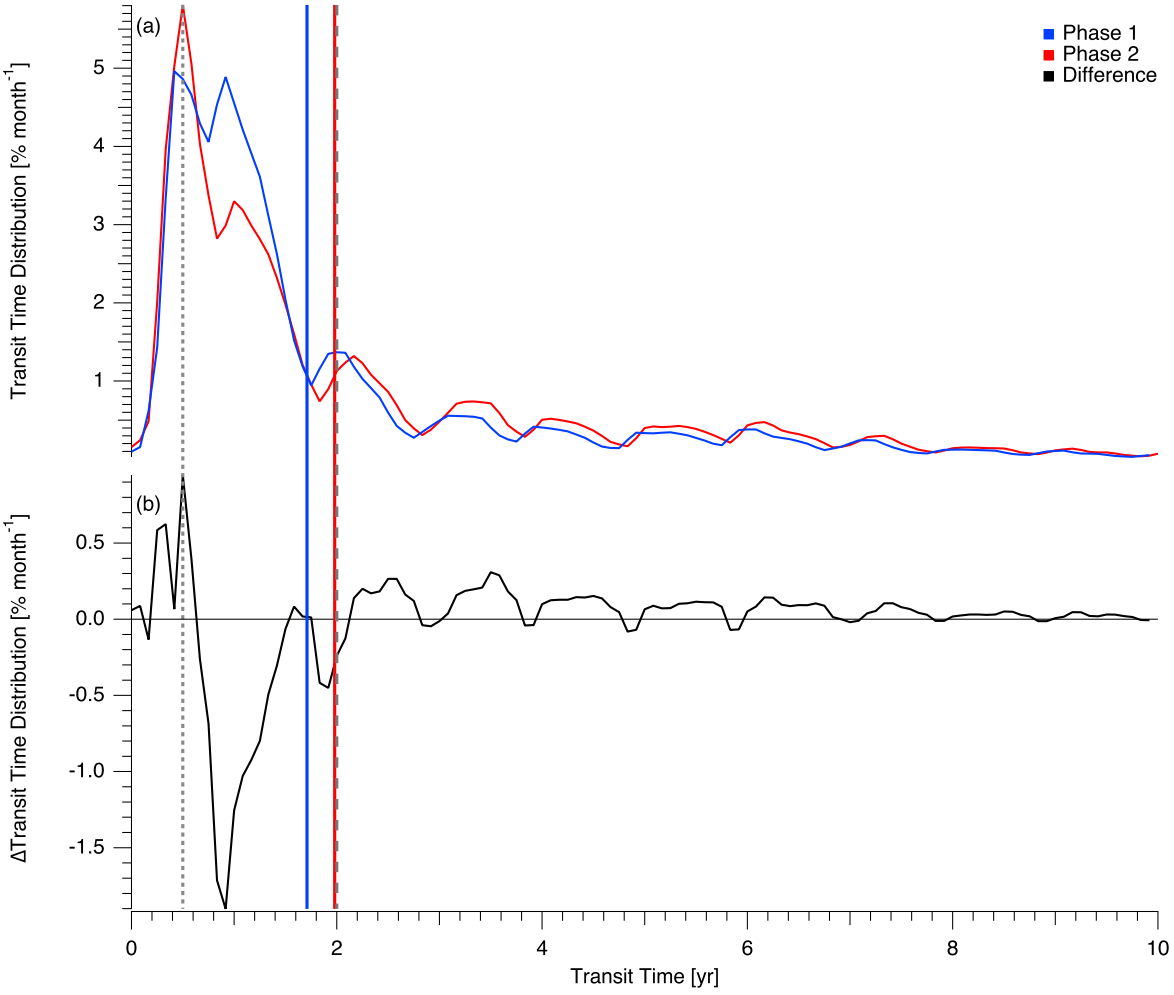

Figure 10. Panel (a): Averaged age spectra simulated by CLaMS for phase 1 (blue) and phase 2 (red). These spectra represent the mean of the individual age spectra available for each data point along the flight track. The mean age is indicated by the respective coloured vertical lines (phase 1: 1.71 years, phase 2: 1.98 years). The difference between both spectra is given in panel (b) showing an enhancement of both, young and old air masses from phase 1 to phase 2. Vertical dashed lines indicate the transit times of six months and 24 months, respectively (see next figures). The bin size of a data point is one month.

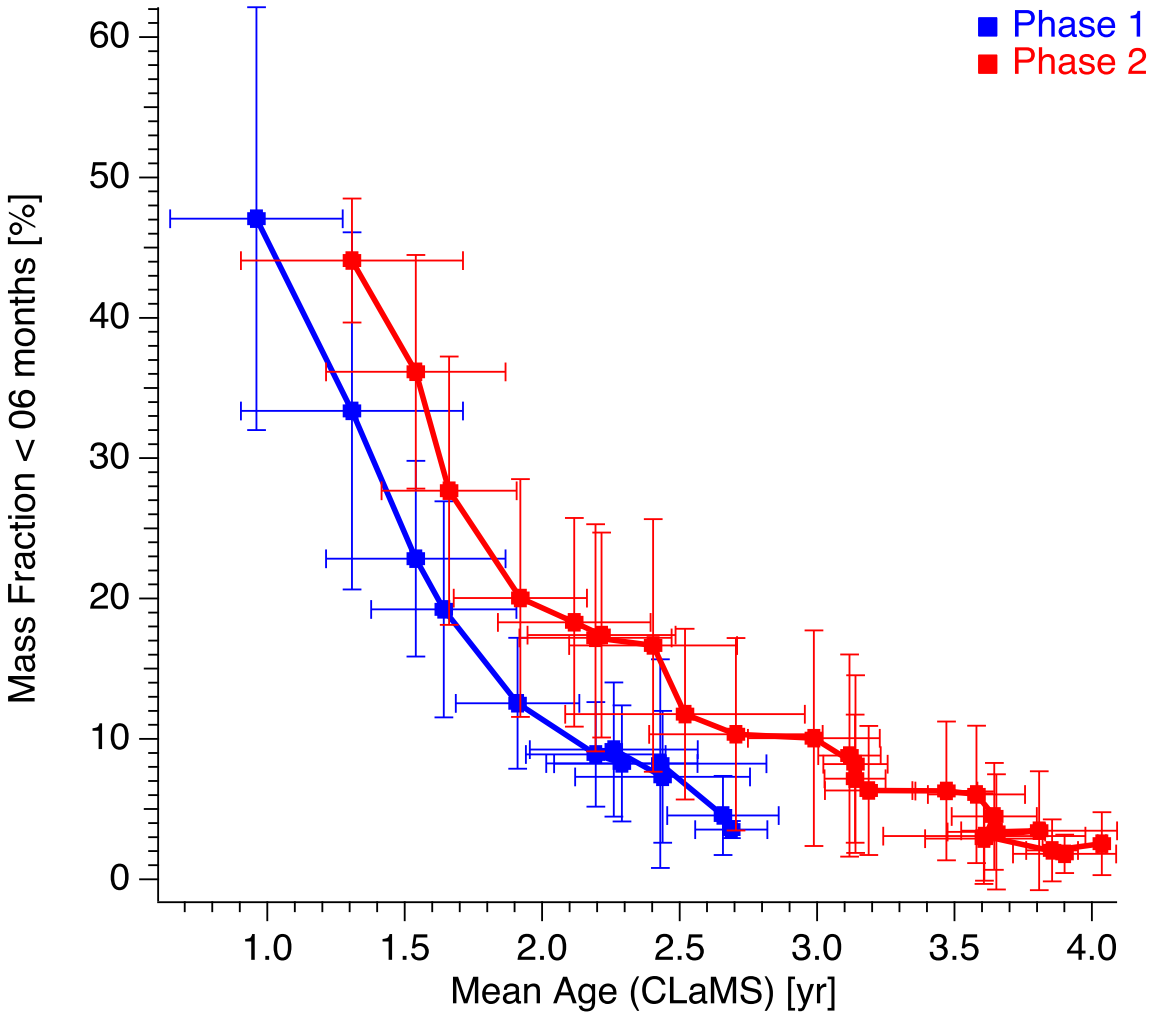

Figure 11. Mean age versus air fractions with transit times < 6 months from the age spectra simulated by CLaMS for phase 1 (blue) and phase 2 (red). Each data point is binned in steps of 5 ppb_V N_2O. The variability in each bin is given by the vertical and horizontal lines, respectively.

contributing to the mean, which however affect the chemical properties of the air parcel by e.g. enhanced mixing of short-lived species. Therefore it is important to account for the full spectral shape when referring to chemical properties of an air mass rather than only the mean age.

During winter 2015/16 CO mixing ratios in the LS increased from January to March while long-lived trace gases denote an ageing of the LS. The analysis of CO-N_2O correlations, the mass balance equation of irreversible mixing and transport transport pathways in the LS and model simulations points towards an increased influence of tropospheric air masses from the tropical lower stratosphere. Additional potential sources of CO in the LS are discussed in the following.

6 Discussion

Since there are different sources for CO at different locations in the atmosphere an increase of carbon monoxide mixing ratios can be due to (i) an increase of isentropic mixing out of the TTL, (ii) an increase of the tropospheric source strength, (iii) a potential influence of the mesosphere and (iv) a change of chemical reaction cycles due to higher amounts of reactive chlorine in the stratosphere. As already discussed the increase of enhanced tropospheric source emissions (ii) is highly unlikely (see Fig. 7). Since our analysis points to an increase of isentropic mixing out of the TTL (i), the possible influence of points (iii) and (iv) have to be further discussed.

Carbon monoxide is produced in the mesosphere due to the photo-dissociation of carbon dioxide. Therefore the composition of mesospheric air masses is clearly distinct from air mass composition of the stratosphere. Rinsland et al. (e.g. 1999) found increased CO mixing ratios up to 90 ppb_V at altitudes around 25 km or $\Theta = 630 - 670$ K and Engel et al. (2006b) found CO values of 600 ppb_V at an altitude of 32 km. Both studies show very low N_2O mixing ratios (< 50 ppb_V). Although the authors found layers of mesospheric air descending down to 22 km, this is not evident for the Arctic winter 2015/16 and lowest N_2O mixing ratios are found to be in the order of 200 ppb_V. This is reflected in the MLS observations that determine the CLaMS upper boundary at $\Theta = 900$ K potential temperature (Fig. 12). The simulation indicates the expected downward transport of mesospheric influenced air, but down to $\Theta = 600$ K at the end of March 2016 in agreement with our observations. CO values minimize at the highest flight levels and equivalent latitudes.

Furthermore, an additional influence of descended mesospheric air into the lower stratosphere would lead to mixing lines very strongly differing from the observed relationship (see Fig. 6), which is not observed in agreement with the CLaMS N_2O-CO scatter plot (Fig. 9).

In general, another important source of carbon monoxide in the atmosphere is the reaction of methane with reactive chlorine, which is not significant in the lower stratosphere (Flocke et al., 1999). However, air masses enriched in reactive chlorine could have been transported downwards, providing potential reactants for the chemical production of CO. Therefore, we simulated the CO yield from the reactions of CH_4 with chlorine, OH and $O(^1D)$ using CLaMS simulations in the box model mode. A large number of air parcel backward trajectories were calculated starting on 15 March from locations within the vortex core (equivalent latitude > 65 °N; potential temperature between $\Theta = 350$ K and $\Theta = 500$ K). Trajectories end on 15 January and

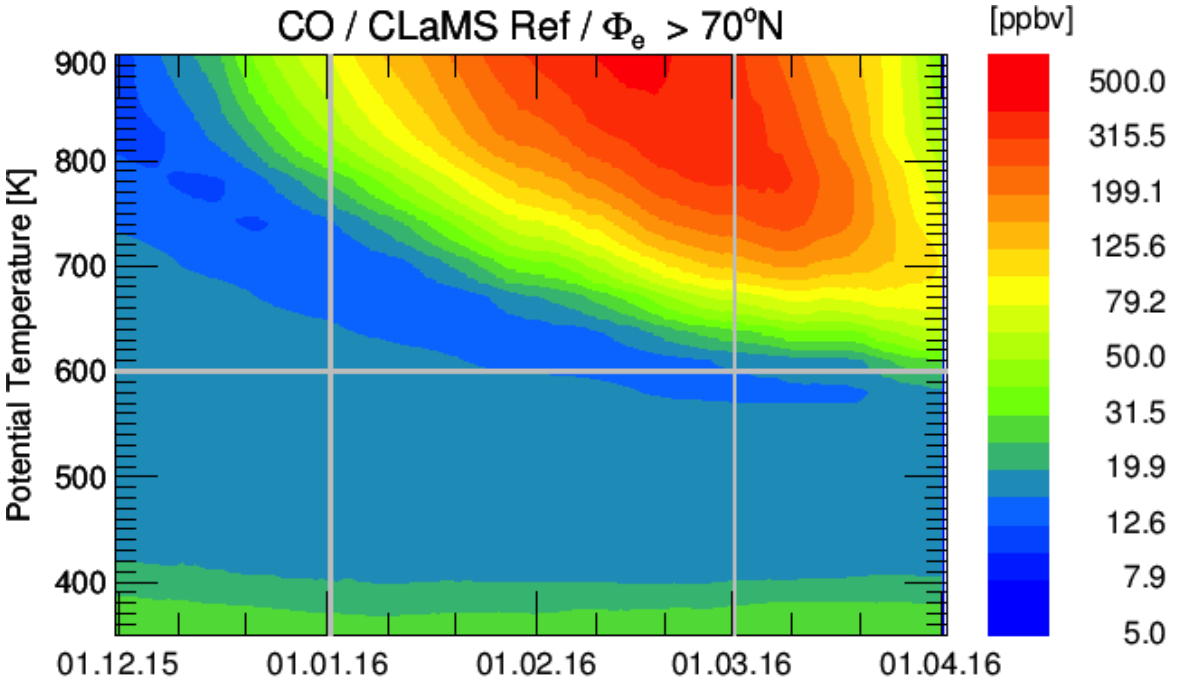

Figure 12. Temporal evolution of zonal mean CO for equivalent latitudes > 70 °N simulated by CLaMS for winter 2015/2016.

chemical composition changes using the CLaMS chemistry module running forward in time for a subset of the trajectories with equivalent latitudes greater 50 °N on 15 January (21480 trajectories). Figure 13 shows the statistical evaluation of the net CO change due to chemistry over the period as function of potential temperature on 15 March. The blue line represents the statistical mean and the dashed lines the 1-σ standard deviation. The mean overall change is even negative over the entire profile, which is due to the oxidation of the produced CO by the reaction with OH. Therefore we conclude that the observed increase of CO in phase 2 is not due to the additional chemical source reaction. The significant increase of air masses younger than six months (Fig.11) also indicates a strong contribution of young rather than mesospheric air.

Figure 13 shows the statistical evaluation of the net CO change due to chemistry over the period as function of potential temperature on 15 March. The blue line represents the statistical mean and the dashed lines the 1-σ standard deviation. As is evident the mean overall change is even negative over the entire profile, which is due to the oxidation of the produced CO by the reaction with OH. Therefore we conclude that the observed increase of CO in phase 2 is not due to the additional chemical source reaction.

To investigate if transport and increased mixing of air mass fractions with transit times smaller than six months in winter 2015/16 was special compared to other years we analysed the climatology of these fractions from 2004 to 2016 and compared it to the calculated fractions in winter 2016, both from the CLaMS model (Fig. 14). The colour code represents the fractions of

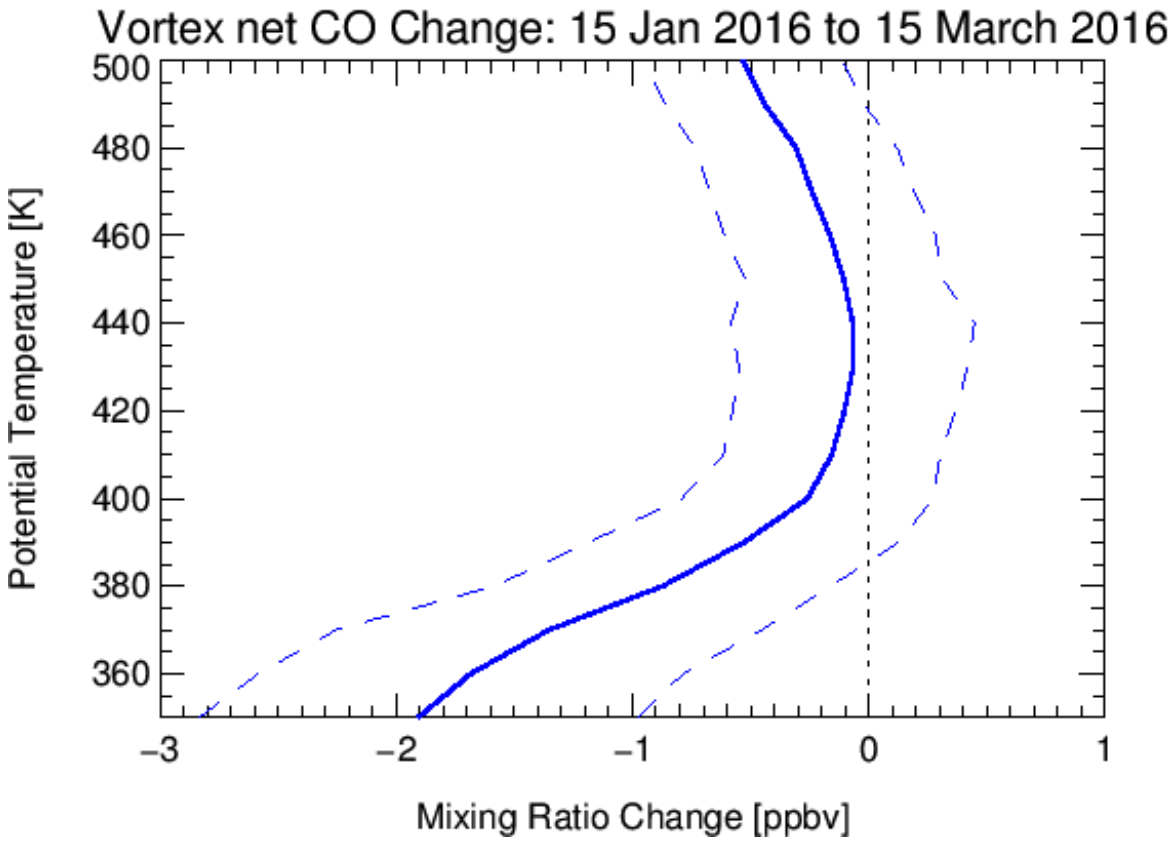

Figure 13. Net change of CO from January to March for air masses in the Arctic vortex (equivalent latitude > 65 °N) due to chemical reactions in the stratosphere and mesosphere calculated by CLaMS. The blue line represents the statistical mean, the dashed lines the 1-σ standard deviation.

air masses with transit times smaller than six months, the contour lines represent the mean age and the thick black line indicates the WMO tropopause.

The climatology shows that the largest fraction of air masses with transit times smaller than six months exceeding 73% is found between the equator and 30 °N up to $\Theta = 430$ K. In January this strong signal has a sharp gradient at $\Theta = 450$ K. These air fractions are transported from January to March to the poles. As a result northward of 70 °N the fraction of air masses with transit times smaller than six months increases by 5% between $\Theta = 360$ K and $\Theta = 420$ K. From January 2016 to March 2016 this transport is even stronger than in the climatology, as shown by the different horizontal gradients in Fig. 14. The mean age in March compared to January at $\Theta = 400$ K shows a higher value in both, the climatology as well as the winter 2015/2016, whereas the structure of the mean age contours show a more horizontal meridional gradient in the winter 2016 compared to the climatology.

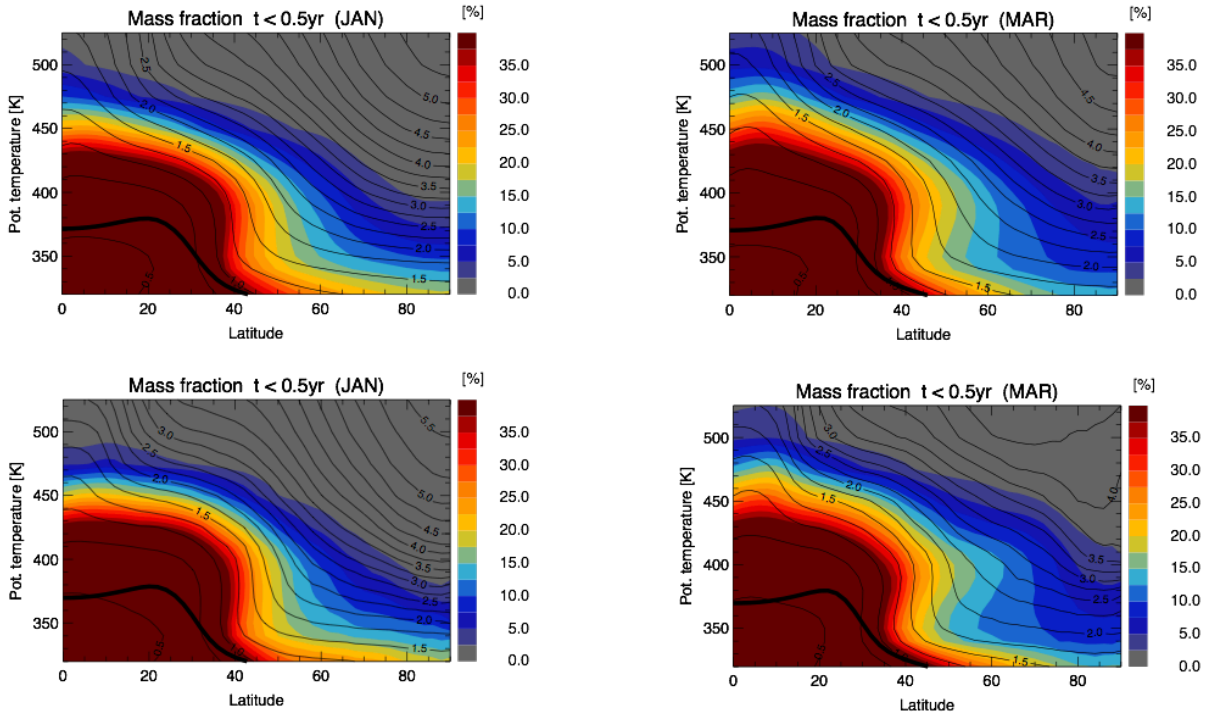

Figure 14. Zonal mean of air mass fractions (colour code) with transit times < 0.5 years for January (left) and March (right) from 2004 to 2016 climatology (upper row) and for 2016 only (lower row) against potential temperature. The contour lines show mean age in years and the thick black line the WMO tropopause.

Finally, these findings highlight the role of mixing of young air in the lower stratosphere of the polar Arctic region with an underlying increase of mean age of air indicating downward transported air masses of older air fractions. The enhanced transport of young air is evident from the climatology and turn out to be particularly strong in the winter 2016.

7 Summary

We present tracer measurements of CO and N_2O measured during the POLSTRACC campaign in winter 2015/16 on board the German HALO research aircraft. The winter 2015/16 was characterised by an extreme cold and stable polar vortex which broke up due to an MFW on 5. March 2016. In combination with measurements of SF_6 and model simulations by the CLaMS model it was possible to analyse the contributions of diabatic transport and isentropic mixing in the UTLS region. The mixing ratios of the long-lived trace gases N_2O and SF_6 decreased over the course of winter and therefore denoted an overall ageing due to subsiding air masses in the Arctic polar lower stratosphere. The calculated mean age based on measured SF_6 shows an ageing of 0.29 years (see Fig. 3 (c)) and for CLaMS 0.27 years (see Fig. 10 (a)), respectively. Remarkably, the short-lived species CO increases at the same time. Since mixing can be identified by tracer-tracer correlations we used CO-N_2O correlations to

quantify the relation between transport and chemistry. Our analysis shows an increase by 3.7 ppb_V CO relative to N_2O, which can be linked to an increase by 6.8 % of mixed air masses out of the TTL region. The comparison with the CLaMS model shows a very good agreement between measurements and model calculations. The CO-N_2O correlation is well reproduced by the model. Analysis of the averaged age spectrum for the respective phase shows that there is a simultaneous increase of fractions of air with transit times larger than two years and fractions of air with transit times smaller than six months. Since the mean age itself is most sensitive to changes on the old tail of the age spectrum, the ageing of air masses in the LS over the course of winter can be explained by the increase of old air masses, characterised by low N_2O and SF_6 measurements. Increased mixing of young air masses adds to this and leads to an increased fraction of the younger part of the age spectrum, consistent with the observed increase of CO. It is evident that this enhancement is due to stronger mixing processes out of the TTL region, where fresh tropospheric air is mixed into the polar lower stratosphere. Other potential sources of CO like mesospheric air and chemical reaction of CH_4 with chlorine are unlikely to have caused the observed increase of CO.

Therefore we conclude that the Arctic lower stratosphere in March was strongly affected by mixing with young tropospheric air, which partly compensates for the overall ageing. These aged air masses are isentropically mixed with younger air masses out of the TTL region. The observations are in-line with the climatology of mixing from 2004-2015 on the basis of Era-interim by the CLaMS model and highlight the importance of horizontal mixing from the tropics for the Arctic winter UTLS.

Author contributions. Jens Krause carried out the measurements and analysed the data with the help of Peter Hoor. Felix Plöger and Jens-Uwe Grooß did the model simulations with the CLaMS model. Andreas Engel, Harald Bönisch and Timo Keber provided the measurement data of SF_6 and mean age. Peter Hoor, Andreas Engel, Felix Plöger and Jens-Uwe Grooß provided helpful discussions and comments. Jens Krause and Peter Hoor wrote the manuscript. Hermann Oelhaf, Björn-Martin Sinnhuber and Wolfgang Woiwode coordinated the POLSTRACC project.

Acknowledgements. This work was supported by the Deutsche Forschungsgemeinschaft (DFG, FKZ EN 367/13-1 and EN 367/11) and the Johannes Gutenberg-University Mainz (FKZ 8585084).

Jens Krause was partly funded under DFG grant HO 4225/7-1.

AGAGE is supported principally by NASA (USA) grants to MIT and SIO, and also by: DECC (UK) and NOAA (USA) grants to Bristol University; CSIRO and BoM (Australia): FOEN grants to Empa (Switzerland); NILU (Norway); SNU (Korea); CMA (China); NIES (Japan); and Urbino University (Italy).

References

Abalos, M., Randel, W. J., Kinnison, D. E., and Serrano, E.: Quantifying tracer transport in the tropical lower stratosphere using WACCM, Atmospheric Chemistry and Physics, 13, 10 591–10 607, doi:10.5194/acp-13-10591-2013, https://www.atmos-chem-phys.net/13/10591/2013/, 2013.

Andrews, A., Boering, K. a., Daube, B. C., Wofsy, S. C., Loewenstein, M., Jost, H., Podolske, J. R., Webster, C. R., Herman, R. L., Scott, D. C., Flesch, G. J., Moyer, E. J., Elkins, J. W., Dutton, G. S., Hurst, D. F., Moore, F. L., Ray, E. a., Romashkin, P. a., and Strahan, S. E.: Mean ages of stratospheric air derived from in situ observations of CO2 , CH4 , and N2O, J. Geophys. Res. Atmos., 106, 32 295–32 314, doi:10.1029/2001JD000465, http://doi.wiley.com/10.1029/2001JD000465, 2001.

Andrews, A. E., Boering, K. A., Daube, B. C., Wofsy, S. C., Hintsa, E. J., Weinstock, E. M., and Bui, T. P.: Empirical age spectra for the lower tropical stratosphere from in situ observations of CO 2 : Implications for stratospheric transport, 104, 26 581–26 595, doi:10.1029/1999JD900150, http://doi.wiley.com/10.1029/1999JD900150, 1999.

Baldwin, M. P., Gray, L. J., Dunkerton, T. J., Hamilton, K., Haynes, P. H., Randel, W. J., Holton, J. R., Alexander, M. J., Hirota, I., Horinouchi, T., Jones, D. B. A., Kinnersley, J. S., Marquardt, C., Sato, K., and Takahashi, M.: The quasi-biennial oscillation, Rev. Geophys., 39, 179–229, doi:10.1029/1999RG000073, http://doi.wiley.com/10.1029/1999RG000073, 2001.

Birner, T. and Bönisch, H.: Residual circulation trajectories and transit times into the extratropical lowermost stratosphere, Atmos. Chem. Phys., 11, 817–827, doi:10.5194/acp-11-817-2011, 2011.

Boenisch, H., Engel, A., Curtius, J., Birner, T., and Hoor, P.: Quantifying transport into the lowermost stratosphere using simultaneous in-situ measurements of SF_6 and CO_2, Atmospheric Chemistry and Physics, 9, 5905–5919, doi:10.5194/acp-9-5905-2009, 2009.

Brewer, A. W.: Evidence for a world circulation provided by the measurements of helium and water vapor distribution in the stratosphere, Q. J. R. Meteorol. Soc., 75, 351–363, 1949.

Butchart, N.: The Brewer-Dobson circulation, Reviews of Geophysics, 52, 157–184, doi:10.1002/2013RG000448, http://dx.doi.org/10.1002/2013RG000448, 2014.

Chen, S., Wu, R., Chen, W., Yu, B., and Cao, X.: Genesis of westerly wind bursts over the equatorial western Pacific during the onset of the strong 2015-2016 El Niño, Atmos. Sci. Lett., 17, 384–391, doi:10.1002/asl.669, http://doi.wiley.com/10.1002/asl.669, 2016.

Dee, D. P., Uppala, S. M., Simmons, A. J., Berrisford, P., Poli, P., Kobayashi, S., Andrae, U., Balmaseda, M. A., Balsamo, G., Bauer, P., Bechtold, P., Beljaars, A. C. M., van de Berg, L., Bidlot, J., Bormann, N., Delsol, C., Dragani, R., Fuentes, M., Geer, A. J., Haimberger, L., Healy, S. B., Hersbach, H., Hólm, E. V., Isaksen, L., Kållberg, P., Köhler, M., Matricardi, M., McNally, A. P., Monge-Sanz, B. M., Morcrette, J.-J., Park, B.-K., Peubey, C., de Rosnay, P., Tavolato, C., Thépaut, J.-N., and Vitart, F.: The ERA-Interim reanalysis: configuration and performance of the data assimilation system, Quarterly Journal of the Royal Meteorological Society, 137, 553–597, doi:10.1002/qj.828, http://dx.doi.org/10.1002/qj.828, 2011.

Dils, B., De Mazière, M., Müller, J. F., Blumenstock, T., Buchwitz, M., de Beek, R., Demoulin, P., Duchatelet, P., Fast, H., Frankenberg, C., Gloudemans, A., Griffith, D., Jones, N., Kerzenmacher, T., Kramer, I., Mahieu, E., Mellqvist, J., Mittermeier, R. L., Notholt, J., Rinsland, C. P., Schrijver, H., Smale, D., Strandberg, A., Straume, A. G., Stremme, W., Strong, K., Sussmann, R., Taylor, J., van den Broek, M., Velazco, V., Wagner, T., Warneke, T., Wiacek, A., and Wood, S.: Comparisons between SCIAMACHY and ground-based FTIR data for total columns of CO, CH_4, CO_2 and N_2O, Atmospheric Chemistry and Physics, 6, 1953–1976, doi:10.5194/acp-6-1953-2006, http://www.atmos-chem-phys.net/6/1953/2006/, 2006.

Dobson, G. M. B.: Origin and Distribution of the Polyatomic Molecules in the Atmosphere, Proceedings of the Royal Society of London A: Mathematical, Physical and Engineering Sciences, 236, 187–193, doi:10.1098/rspa.1956.0127, http://rspa.royalsocietypublishing.org/content/236/1205/187, 1956.

Ehhalt, D. H., Rohrer, F., Blake, D. R., Kinnison, D. E., and Konopka, P.: On the use of nonmethane hydrocarbons for the determination of age spectra in the lower stratosphere, J. Geophys. Res. Atmos., 112, 1–12, doi:10.1029/2006JD007686, 2007.

Engel, A., Strunk, M., Müller, M., Haase, H.-P., Poss, C., Levin, I., and Schmidt, U.: Temporal development of total chlorine in the high-latitude stratosphere based on reference distributions of mean age derived from CO2 and SF6, Journal of Geophysical Research: Atmospheres, 107, ACH 1–1–ACH 1–11, doi:10.1029/2001JD000584, http://dx.doi.org/10.1029/2001JD000584, 2002.

Engel, A., Bönisch, H., Brunner, D., Fischer, H., Franke, H., Gunther, G., Gurk, C., Hegglin, M., Hoor, P., Konigstedt, R., Krebsbach, M., Maser, R., Parchatka, U., Peter, T., Schell, D., Schiller, C., Schmidt, U., Spelten, N., Szabo, T., Weers, U., Wernli, H., Wetter, T., and Wirth, V.: Highly resolved observations of trace gases in the lowermost stratosphere and upper troposphere from the Spurt project: an overview, Atmos. Chem. Phys., 6, 283–301, doi:10.5194/acp-6-283-2006, 2006a.

Engel, A., Möbius, T., Haase, H.-P., Bönisch, H., Wetter, T., Schmidt, U., Levin, I., Reddmann, T., Oelhaf, H., Wetzel, G., Grunow, K., Huret, N., and Pirre, M.: Observation of mesospheric air inside the arctic stratospheric polar vortex in early 2003, Atmospheric Chemistry and Physics, 6, 267–282, doi:10.5194/acp-6-267-2006, http://www.atmos-chem-phys.net/6/267/2006/, 2006b.

Engel, A., Möbius, T., Bönisch, H., Schmidt, U., Heinz, R., Levin, I., Atlas, E., Aoki, S., Nakazawa, T., Sugawara, S., Moore, F., Hurst, D., Elkins, J., Schauffler, S., Andrews, A., and Boering, K.: Age of stratospheric air unchanged within uncertainties over the past 30 years, Nat. Geosci., 2, 28–31, doi:10.1038/ngeo388, http://dx.doi.org/10.1038/ngeo388, 2009.

Fischer, H., Wienhold, F. G., Hoor, P., Bujok, O., Schiller, C., Siegmund, P., Ambaum, M., Scheeren, H. A., and Lelieveld, J.: Tracer correlations in the northern high latitude lowermost stratosphere: Influence of cross-tropopause mass exchange, Geophysical Research Letters, 27, 97–100, doi:10.1029/1999GL010879, http://dx.doi.org/10.1029/1999GL010879, 2000.

Fix, A., Amediek, A., Ehret, G., Groß, S., Kiemle, C., Reitebuch, O., and Wirth, M.: On the benefit of airborne demonstrators for space borne lidar missions, in: International Conference on Space Optics, 2016.

Flocke, F., Herman, R., and Salawitch, R.: An examination of chemistry and transport processes in the tropical lower stratosphere using observations of long-lived and short-lived compounds obtained during STRAT and POLARIS, J. Geophys. Res., 104, 26 625–26 642, doi:10.1029/1999JD900504, 1999.

Friedl-Vallon, F., Gulde, T., Hase, F., Kleinert, A., Kulessa, T., Maucher, G., Neubert, T., Olschewski, F., Piesch, C., Preusse, P., Rongen, H., Sartorius, C., Schneider, H., Schönfeld, A., Tan, V., Bayer, N., Blank, J., Dapp, R., Ebersoldt, A., Fischer, H., Graf, F., Guggenmoser, T., Höpfner, M., Kaufmann, M., Kretschmer, E., Latzko, T., Nordmeyer, H., Oelhaf, H., Orphal, J., Riese, M., Schardt, G., Schillings, J., Sha, M. K., Suminska-Ebersoldt, O., and Ungermann, J.: Instrument concept of the imaging Fourier transform spectrometer GLORIA, Atmospheric Measurement Techniques, 7, 3565–3577, doi:10.5194/amt-7-3565-2014, https://www.atmos-meas-tech.net/7/3565/2014/, 2014.

Fueglistaler, S., Dessler, A. E., Dunkerton, T. J., Folkins, I., Fu, Q., and Mote, P. W.: Tropical tropopause layer, Reviews of Geophysics, 47, doi:10.1029/2008RG000267, http://dx.doi.org/10.1029/2008RG000267, 2009.

Garny, H., Birner, T., Bönisch, H., and Bunzel, F.: The effects of mixing on age of air, J. Geophys. Res. Atmos., 119, 7015–7034, doi:10.1002/2013JD021417, http://doi.wiley.com/10.1002/2013JD021417, 2014.

Grooß, J.-U., Engel, I., Borrmann, S., Frey, W., Günther, G., Hoyle, C. R., Kivi, R., Luo, B. P., Molleker, S., Peter, T., Pitts, M. C., Schlager, H., Stiller, G., Vömel, H., Walker, K. A., and Müller, R.: Nitric acid trihydrate nucleation and denitrification in the Arctic stratosphere,

Atmospheric Chemistry and Physics, 14, 1055–1073, doi:10.5194/acp-14-1055-2014, https://www.atmos-chem-phys.net/14/1055/2014/, 2014.

Haenel, F. J., Stiller, G. P., von Clarmann, T., Funke, B., Eckert, E., Glatthor, N., Grabowski, U., Kellmann, S., Kiefer, M., Linden, A., and Reddmann, T.: Reassessment of MIPAS age of air trends and variability, Atmos. Chem. Phys., 15, 13 161–13 176, doi:10.5194/acp-15-13161-2015, http://www.atmos-chem-phys.net/15/13161/2015/, 2015.

Hall, T. M. and Plumb, R. A.: Age as a diagnostic of stratospheric transport, Journal of Geophysical Research: Atmospheres, 99, 1059–1070, doi:10.1029/93JD03192, http://dx.doi.org/10.1029/93JD03192, 1994.

Hall, T. M. and Waugh, D. W.: Timescales for the stratospheric circulation derived from tracers, jgr, 102, 8991–9001, doi:10.1029/96JD03713, 1997.

Hartmann, D. J., Klein Tank, A. M. G., Rusticucci, M., Alexander, L. V., Brönnimann, S., Charabi, Y. A.-R., Dentener, F. J., Dlugokencky, E. J., Easterling, D. R., Kaplan, A., Soden, B. J., Thorne, P. W., Wild, M., and Zhai, P.: Observations: Atmosphere and Surface, Clim. Chang. 2013 Phys. Sci. Basis. Contrib. Work. Gr. I to Fifth Assess. Rep. Intergov. Panel Clim. Chang., pp. 159–254, doi:10.1017/CBO9781107415324.008, http://www.climatechange2013.org/report/full-report/, 2013.

Haynes, P. and Shuckburgh, E.: Effective diffusivity as a diagnostic of atmospheric transport: 1. Stratosphere, J. Geophys. Res., 105, 22 777, doi:10.1029/2000JD900093, http://doi.wiley.com/10.1029/2000JD900093, 2000.

Haynes, P. H., McIntyre, M. E., Shepherd, T. G., Marks, C. J., and Shine, K. P.: On the "Downward Control" of Extratropical Diabatic Circulations by Eddy-Induced Mean Zonal Forces, Journal of the Atmospheric Sciences, 48, 651–678, doi:10.1175/1520-0469, 1991.

Hegglin, M. and Shepherd, T.: O3-N2O correlations from the Atmospheric Chemistry Experiment: Revisiting a diagnostic of transport and chemistry in the stratosphere, J. Geophys. Res., 112, 1–15, doi:10.1029/2006JD008281, 2007.

Hegglin, M. I., Brunner, D., Peter, T., Hoor, P., Fischer, H., Staehelin, J., Krebsbach, M., Schiller, C., Parchatka, U., and Weers, U.: Measurements of NO, NO_y, N_2O, and O_3 during SPURT: implications for transport and chemistry in the lowermost stratosphere, Atmospheric Chemistry and Physics, 6, 1331–1350, doi:10.5194/acp-6-1331-2006, http://www.atmos-chem-phys.net/6/1331/2006/, 2006.

Herman, R., Webster, C., May, R., Scott, D., Hu, H., Moyer, E., Wennberg, P., Hanisco, T., Lanzendorf, E., Salawitch, R., Yung, Y., Margitan, J., and Bui, T.: Measurements of {CO} in the upper troposphere and lower stratosphere, Chemosphere - Global Change Science, 1, 173 – 183, doi:https://doi.org/10.1016/S1465-9972(99)00008-2, http://www.sciencedirect.com/science/article/pii/S1465997299000082, 1999.

Holton: An introduction to dynamic meteorology, Elsevier Academic Press, 2004.

Holton, J., Haynes, P., and Mcintyre, M.: Stratosphere-Troposphere Exchange, Rev. Geophys., 33,4, 403–439, 1995.

Holton, J. R. and Tan, H.-C.: The Influence of the Equatorial Quasi-Biennial Oscillation on the Global Circulation at 50 mb, doi:10.1175/1520-0469, 1980.

Hoor, P., Fischer, H., Lange, L., Lelieveld, J., and Brunner, D.: Seasonal variations of a mixing layer in the lowermost stratosphere as identified by the CO-O3 correlation from in situ measurements, Journal of Geophysical Research: Atmospheres, 107, 1–1 – 1–11, doi:10.1029/2000JD000289, http://dx.doi.org/10.1029/2000JD000289, 2002.

Hoor, P., Gurk, C., Brunner, D., Hegglin, M. I., Wernli, H., and Fischer, H.: Seasonality and extent of extratropical TST derived from in-situ CO measurements during SPURT, Atmospheric Chemistry and Physics, 4, 1427–1442, doi:10.5194/acp-4-1427-2004, http://www.atmos-chem-phys.net/4/1427/2004/, 2004.

Hoor, P., Fischer, H., and Lelieveld, J.: Tropical and extratropical tropospheric air in the lowermost stratosphere over Europe: A CO-based budget, Geophysical Research Letters, 32, doi:10.1029/2004GL022018, http://dx.doi.org/10.1029/2004GL022018, 2005.

Hoor, P., Wernli, H., Hegglin, M. I., and Bönisch, H.: Transport timescales and tracer properties in the extratropical UTLS, Atmospheric Chemistry and Physics, 10, 7929–7944, doi:10.5194/acp-10-7929-2010, http://www.atmos-chem-phys.net/10/7929/2010/, 2010.

Hoskins, B. J.: Towards a PV-theta view of the general circulation, Tellus A, 43, 27–35, doi:10.1034/j.1600-0870.1991.t01-3-00005.x, http://adsabs.harvard.edu/abs/1991TellA..43...27Hhttp://tellusa.net/index.php/tellusa/article/view/11936, 1991.

Kaufmann, M., Blank, J., Guggenmoser, T., Ungermann, J., Engel, A., Ern, M., Friedl-Vallon, F., Gerber, D., Grooß, J. U., Guenther, G., Höpfner, M., Kleinert, A., Kretschmer, E., Latzko, T., Maucher, G., Neubert, T., Nordmeyer, H., Oelhaf, H., Olschewski, F., Orphal, J., Preusse, P., Schlager, H., Schneider, H., Schuettemeyer, D., Stroh, F., Suminska-Ebersoldt, O., Vogel, B., M. Volk, C., Woiwode, W., and Riese, M.: Retrieval of three-dimensional small-scale structures in upper-tropospheric/lower-stratospheric composition as measured by GLORIA, Atmospheric Measurement Techniques, 8, 81–95, doi:10.5194/amt-8-81-2015, http://www.atmos-meas-tech.net/8/81/2015/, 2015.

Ko, M. K. W., Newman, P. A., Reimann, S., and Strahan, S. E.: SPARC Report, No. 6, 256 pp., http://www.sparc-climate.org/publications/sparc-reports/, 2013.

Konopka, P., Steinhorst, H.-M., Grooß, J.-U., Günther, G., Müller, R., Elkins, J. W., Jost, H.-J., Richard, E., Schmidt, U., Toon, G., and McKenna, D. S.: Mixing and ozone loss in the 1999–2000 Arctic vortex: Simulations with the three-dimensional Chemical Lagrangian Model of the Stratosphere (CLaMS), Journal of Geophysical Research: Atmospheres, 109, doi:10.1029/2003JD003792, http://dx.doi.org/10.1029/2003JD003792, 2004.

L'Heureux, M. L., Takahashi, K., Watkins, A. B., Barnston, A. G., Becker, E. J., Di Liberto, T. E., Gamble, F., Gottschalck, J., Halpert, M. S., Huang, B., Mosquera-Vásquez, K., and Wittenberg, A. T.: Observing and Predicting the 2015/16 El Niño, Bull. Am. Meteorol. Soc., 98, 1363–1382, doi:10.1175/BAMS-D-16-0009.1, http://journals.ametsoc.org/doi/10.1175/BAMS-D-16-0009.1, 2017.

Manney, G. L. and Lawrence, Z. D.: The major stratospheric final warming in 2016: Dispersal of vortex air and termination of Arctic chemical ozone loss, Atmos. Chem. Phys. Discuss., pp. 1–40, doi:10.5194/acp-2016-633, http://www.atmos-chem-phys-discuss.net/acp-2016-633/, 2016.

Marcy, T., Popp, P., Gao, R., Fahey, D., Ray, E., Richard, E., Thompson, T., Atlas, E., Loewenstein, M., Wofsy, S., Park, S., Weinstock, E., Swartz, W., and Mahoney, M.: Measurements of trace gases in the tropical tropopause layer, Atmospheric Environment, 41, 7253–7261, doi:10.1016/j.atmosenv.2007.05.032, 2007.

Matthias, V., Dörnbrack, A., and Stober, G.: The extraordinarily strong and cold polar vortex in the early northern winter 2015/2016, Geophysical Research Letters, 43, 12,287–12,294, doi:10.1002/2016GL071676, http://dx.doi.org/10.1002/2016GL071676, 2016.

McKenna, D. S., Konopka, P., Grooß, J.-U., Günther, G., Müller, R., Spang, R., Offermann, D., and Orsolini, Y.: A new Chemical Lagrangian Model of the Stratosphere (CLaMS) 1. Formulation of advection and mixing, Journal of Geophysical Research: Atmospheres, 107, ACH 15–1–ACH 15–15, doi:10.1029/2000JD000114, http://dx.doi.org/10.1029/2000JD000114, 2002.

Müller, S., Hoor, P., Bozem, H., Gute, E., Vogel, B., Zahn, A., Bönisch, H., Keber, T., Krämer, M., Rolf, C., Riese, M., Schlager, H., and Engel, A.: Impact of the Asian monsoon on the extratropical lower stratosphere: trace gas observations during TACTS over Europe 2012, Atmospheric Chemistry and Physics, 16, 10 573–10 589, doi:10.5194/acp-16-10573-2016, http://www.atmos-chem-phys.net/16/10573/2016/, 2016.

Müller, S., Hoor, P., Berkes, F., Bozem, H., Klingebiel, M., Reutter, P., Smit, H. G. J., Wendisch, M., Spichtinger, P., and Borrmann, S.: In situ detection of stratosphere-troposphere exchange of cirrus particles in the midlatitudes, Geophysical Research Letters, 42, 949–955, doi:10.1002/2014GL062556, http://dx.doi.org/10.1002/2014GL062556, 2015.

Newman, P., Coy, L., Pawson, S., and Lait, L. R.: The anomalous change in the QBO in 2015-2016, Geophys. Res. Lett., 43, 8791–8797, doi:10.1002/2016GL070373, 2016.

Niwano, M., Yamazaki, K., and Shiotani, M.: Seasonal and {QBO} variations of ascent rate in the tropical lower stratosphere as inferred from {UARS HALOE} trace gas data, J. Geophys. Res., 108, 4794, doi:10.1029/2003JD003871, 2003.

NOAA: Combined Nitrous Oxide data from the NOAA/ESRL Global Monitoring Division.

Osprey, S. M., Butchart, N., Knight, J. R., Scaife, A. A., Hamilton, K., Anstey, J. A., Schenzinger, V., and Zhang, C.: An unexpected disruption of the atmospheric quasi-biennial oscillation, Science (80-.)., 353, 1424–1427, doi:10.1126/science.aah4156, http://www.sciencemag.org/cgi/doi/10.1126/science.aah4156, 2016.

Palazzi, E., Fierli, F., Stiller, G. P., and Urban, J.: Probability density functions of long-lived tracer observations from satellite in the subtropical barrier region: Data intercomparison, Atmos. Chem. Phys., 11, 10 579–10 598, doi:10.5194/acp-11-10579-2011, 2011.

Palmeiro, F. M., Iza, M., Barriopedro, D., Calvo, N., and García-Herrera, R.: The complex behavior of El Niño winter 2015-2016, Geophys. Res. Lett., 44, 2902–2910, doi:10.1002/2017GL072920, http://doi.wiley.com/10.1002/2017GL072920, 2017.

Pan, L. L., Randel, W. J., Gary, B. L., Mahoney, M. J., and Hintsa, E. J.: Definitions and sharpness of the extratropical tropopause: A trace gas perspective, J. Geophys. Res. D Atmos., 109, 1–11, doi:10.1029/2004JD004982, 2004.

Pan, L. L., Wei, J. C., Kinnison, D. E., Garcia, R. R., Wuebbles, D. J., and Brasseur, G. P.: A set of diagnostic for evaluating chemistry-climate models in the extratropical tropopause region, J. Geophys. Res. Atmos., 112, 1–12, doi:10.1029/2006JD007792, 2007.

Ploeger, F. and Birner, T.: Seasonal and inter-annual variability of lower stratospheric age of air spectra, Atmospheric Chemistry and Physics, 16, 10 195–10 213, doi:10.5194/acp-16-10195-2016, https://www.atmos-chem-phys.net/16/10195/2016/, 2016.

Ploeger, F., Günther, G., Konopka, P., Fueglistaler, S., Müller, R., Hoppe, C., Kunz, A., Spang, R., Grooß, J.-U., and Riese, M.: Horizontal water vapor transport in the lower stratosphere from subtropics to high latitudes during boreal summer, J. Geophys. Res. Atmos., 118, 8111–8127, doi:10.1002/jgrd.50636, http://doi.wiley.com/10.1002/jgrd.50636, 2013.

Ploeger, F., Riese, M., Haenel, F., Konopka, P., Müller, R., and Stiller, G.: Variability of stratospheric mean age of air and of the local effects of residual circulation and eddy mixing, Journal of Geophysical Research: Atmospheres, 120, 716–733, doi:10.1002/2014JD022468, http://dx.doi.org/10.1002/2014JD022468, 2015.

Plumb, R. A.: Stratospheric Transport, Journal of the Meteorological Society of Japan. Ser. II, 80, 793–809, doi:10.2151/jmsj.80.793, 2002.

Pommrich, R., Müller, R., Grooß, J.-U., Konopka, P., Ploeger, F., Vogel, B., Tao, M., Hoppe, C. M., Günther, G., Spelten, N., Hoffmann, L., Pumphrey, H.-C., Viciani, S., D'Amato, F., Volk, C. M., Hoor, P., Schlager, H., and Riese, M.: Tropical troposphere to stratosphere transport of carbon monoxide and long-lived trace species in the Chemical Lagrangian Model of the Stratosphere (CLaMS), Geoscientific Model Development, 7, 2895–2916, doi:10.5194/gmd-7-2895-2014, https://www.geosci-model-dev.net/7/2895/2014/, 2014.

Prinn, R. G., Weiss, R. F., Fraser, P. J., Simmonds, P. G., Cunnold, D. M., Alyea, F. N., O'Doherty, S., Salameh, P., Miller, B. R., Huang, J., Wang, R. H. J., Hartley, D. E., Harth, C., Steele, L. P., Sturrock, G., Midgley, P. M., and McCulloch, A.: A history of chemically and radiatively important gases in air deduced from ALE/GAGE/AGAGE, Journal of Geophysical Research: Atmospheres, 105, 17 751–17 792, doi:10.1029/2000JD900141, http://dx.doi.org/10.1029/2000JD900141, 2000.

Randel, W. J., Wu, F., Vömel, H., Nedoluha, G. E., and Forster, P.: Decreases in stratospheric water vapor after 2001: Links to changes in the tropical tropopause and the Brewer-Dobson circulation, J. Geophys. Res. Atmos., 111, 1–11, doi:10.1029/2005JD006744, 2006.

Ray, E. A., Moore, F. L., Elkins, J. W., Rosenlof, K. H., Laube, J. C., Röckmann, T., Marsh, D. R., and Andrews, A. E.: Quantification of the SF6 lifetime based on mesospheric loss measured in the stratospheric polar vortex, Journal of Geophysical Research: Atmospheres, 122, 4626–4638, doi:10.1002/2016JD026198, http://dx.doi.org/10.1002/2016JD026198, 2017.

Riese, M., Ploeger, F., Rap, A., Vogel, B., Konopka, P., Dameris, M., and Forster, P.: Impact of uncertainties in atmospheric mixing on simulated UTLS composition and related radiative effects, Journal of Geophysical Research: Atmospheres (1984–2012), 117, doi:10.1029/2012JD017751, http:https://dx.doi.org/10.1029/2012JD017751, 2012.

Riese, M., Oelhaf, H., Preusse, P., Blank, J., Ern, M., Friedl-Vallon, F., Fischer, H., Guggenmoser, T., Höpfner, M., Hoor, P., Kaufmann, M., Orphal, J., Plöger, F., Spang, R., Suminska-Ebersoldt, O., Ungermann, J., Vogel, B., and Woiwode, W.: Gimballed Limb Observer for Radiance Imaging of the Atmosphere (GLORIA) scientific objectives, Atmospheric Measurement Techniques, 7, 1915–1928, doi:10.5194/amt-7-1915-2014, https://www.atmos-meas-tech.net/7/1915/2014/, 2014.

Rinsland, C. P., Salawitch, R. J., Gunson, M. R., Solomon, S., Zander, R., Mahieu, E., Goldman, A., Newchurch, M. J., Irion, F. W., and Chang, A. Y.: Polar stratospheric descent of NO y and CO and Arctic denitrification during winter 1992-1993, J. Geophys. Res. Atmos., 104, 1847–1861, doi:10.1029/1998JD100034, http://doi.wiley.com/10.1029/1998JD100034, 1999.

Rosenfield, J. E., Newman, P. A., and Schoeberl, M. R.: Computations of diabatic descent in the stratospheric polar vortex, Journal of Geophysical Research: Atmospheres, 99, 16 677–16 689, doi:10.1029/94JD01156, http://dx.doi.org/10.1029/94JD01156, 1994.

Rosenlof, K., Tuck, A., Kelly, K., Russell, J., and McCormick, M.: Hemispheric asymmetries in water vapor and inferences about transport in the lower stratosphere, J. Geophys. Res., 102, 13 213, doi:10.1029/97JD00873, 1997.

Sala, S., Bönisch, H., Keber, T., Oram, D. E., Mills, G., and Engel, A.: Deriving an atmospheric budget of total organic bromine using airborne in situ measurements from the western Pacific area during SHIVA, Atmospheric Chemistry and Physics, 14, 6903–6923, doi:10.5194/acp-14-6903-2014, http://www.atmos-chem-phys.net/14/6903/2014/, 2014.

Schiller, C., Bozem, H., Gurk, C., Parchatka, U., Königstedt, R., Harris, G., Lelieveld, J., and Fischer, H.: Applications of quantum cascade lasers for sensitive trace gas measurements of CO, CH4, N2O and HCHO, Applied Physics B, 92, 419–430, doi:10.1007/s00340-008-3125-0, http://dx.doi.org/10.1007/s00340-008-3125-0, 2008.

Schoeberl, M., Douglass, A., Polansky, B., Bonne, C., Walker, K., and Bernath, P.: Estimation of stratospheric age spectrum from chemical tracers, J. Geophys. Res. Atmos., 110, 1–18, doi:10.1029/2005JD006125, 2005.

Schoeberl, M. R., Sparling, L. C., Jackman, C. H., and Fleming, E. L.: A Lagrangian view of stratospheric trace gas distributions, J. Geophys. Res. Atmos., 105, 1537–1552, doi:10.1029/1999JD900787, http://doi.wiley.com/10.1029/1999JD900787, 2000.

Schoeberl, M. R., Duncan, B. N., Douglass, A. R., Waters, J., Livesey, N., Read, W., and Filipiak, M.: The carbon monoxide tape recorder, Geophysical Research Letters, 33, n/a–n/a, doi:10.1029/2006GL026178, http://dx.doi.org/10.1029/2006GL026178, 2006.

Solomon, S.: Stratospheric ozone depletion: A review of concepts and history, Rev. Geophys., 37, 275–316, doi:10.1029/1999RG900008, http://doi.wiley.com/10.1029/1999RG900008{%}5Cnfile:///Files/1C/1C8C7992-1164-4AF2-A105-A09A9192890A.pdf{%}5Cnpapers3://publication/doi/10.1029/1999rg900008, 1999.

Stiller, G., von Clarmann, T., Höpfner, M., Glatthor, N., Grabowski, U., Kellmann, S., Kleinert, A., Linden, A., Milz, M., Reddmann, T., Steck, T., Fischer, H., Funke, B., López-Puertas, M., and Engel, A.: Global distribution of mean age of stratospheric air from MIPAS SF₆ measurements, Atmos. Chem. Phys., 8, 677–695, doi:10.5194/acp-8-677-2008, http://www.atmos-chem-phys.net/8/677/2008/, 2008.

Stiller, G., Von Clarmann, T., Haenel, F., Funke, B., Glatthor, N., Grabowski, U., Kellmann, S., Kiefer, M., Linden, A., Lossow, S., and López-Puertas, M.: Observed temporal evolution of global mean age of stratospheric air for the 2002 to 2010 period, Atmos. Chem. Phys., 12, 3311–3331, doi:10.5194/acp-12-3311-2012, 2012.

Strahan, S. E., Loewenstein, M., and Podolske, J. R.: Climatology and small-scale structure of lower stratospheric N2O based on in situ observations, J. Geophys. Res., 104, 2195–2208, doi:10.1029/1998JD200075, 1999.

Waugh, D.: Age of stratospheric air: Theory, observations, and models, Rev. Geophys., 40, 1010, doi:10.1029/2000RG000101, http://www.agu.org/pubs/crossref/2002/2000RG000101.shtml{%}5Cnhttp://doi.wiley.com/10.1029/2000RG000101http://doi.wiley.com/10.1029/2000RG000101, 2002.

Waugh, D. W., Plumb, R. A., Elkins, J. W., Fahey, D. W., Boering, K. A., Dutton, G. S., Volk, C. M., Keim, E., Gao, R.-S., Daube, B. C., Wofsy, S. C., Loewenstein, M., Podolske, J. R., Chan, K. R., Proffitt, M. H., Kelly, K. K., Newman, P. A., and Lait, L. R.: Mixing of polar vortex air into middle latitudes as revealed by tracer-tracer scatterplots, Journal of Geophysical Research: Atmospheres, 102, 13 119–13 134, doi:10.1029/96JD03715, http://dx.doi.org/10.1029/96JD03715, 1997.

Wirth, M., Fix, A., Mahnke, P., Schwarzer, H., Schrandt, F., and Ehret, G.: The airborne multi-wavelength water vapor differential absorption lidar WALES: system design and performance, Applied Physics B, 96, 201, doi:10.1007/s00340-009-3365-7, http://dx.doi.org/10.1007/s00340-009-3365-7, 2009.

Zahn, A., Brenninkmeijer, C. A. M., Maiss, M., Scharffe, D. H., Crutzen, P. J., Hermann, M., Heintzenberg, J., Wiedensohler, A., Güsten, H., Heinrich, G., Fischer, H., Cuijpers, J. W. M., and van Velthoven, P. F. J.: Identification of extratropical two-way troposphere-stratosphere mixing based on CARIBIC measurements of O3, CO, and ultrafine particles, Journal of Geophysical Research: Atmospheres, 105, 1527–1535, doi:10.1029/1999JD900759, http://dx.doi.org/10.1029/1999JD900759, 2000.